THE ROLE OF IRON CHELATION IN PULMONARY INFLAMMATION

by

Nazli Alizadeh-Tabrizi

Submitted in partial fulfilment of the requirements
for the degree of Master of Science

at

Dalhousie University
Halifax, Nova Scotia
August 2021

I dedicate this thesis to my beloved parents

Tayyebeh Bahreinian and Behrooz Alizadeh Tabrizi

TABLE OF CONTENTS

LIST OF TABLES vi

LIST OF FIGURES vii

ABSTRACT viii

LIST OF ABBREVIATIONS USED ix

ACKNOWLEGMENTS xiv

Chapter 1: Introduction 1

1.1. Lung Physiology 1

1.1.1. Respiratory function 1

1.1.2. Immunological function 2

1.2. Lung Inflammation 4

1.2.1. Endotoxin structure 5

1.2.2. Endotoxin response 7

1.2.3. Endotoxin types 9

1.3. Iron Physiology 10

1.3.1. Systemic iron homeostasis 11

1.3.2. Pulmonary iron regulation 13

1.4. Iron in lung inflammation 14

1.5. Iron chelation 16

1.6. Hypothesis 18

1.7. Objectives 18

Chapter 2: Materials and Methods 19

2.1. Animals 19

2.2. Experimental Model 19

2.2.1. Anesthesia 19
2.2.2. LPS instillation 20
2.2.3. Experimental Groups 21
2.3. Histology 23
2.4. Western blotting 24
2.4.1. Protein extraction for western blotting 24
2.4.2. Bradford protein assay 24
2.4.3. SDS-PAGE electrophoresis 25
2.5. Lung tissue inflammatory mediators 27
2.5.1. Protein extraction for multiplex assay 28
2.5.2. Protein assay for multiplex assays 29
2.6. Plasma inflammatory mediators 29
2.7. Statistical analysis 29
Chapter 3: Results 30
3.1. Objective 1: Establish murine lung inflammatory model by intranasal instillation of LPS 30
3.1.1. Histology 30
3.1.2. NF-κB activation by LPS 34
3.1.3. Lung cytokines 36
3.1.4. Plasma cytokines 40
3.2. Objective 2: Study the effects of iron chelation by DIBI on the inflammatory markers of lung inflammation established in Objective 1 43
3.2.1. Histology 43
3.2.2. NF-κB activation by LPS and effect of DIBI treatment 48
3.2.3. Lung cytokine levels in presence of DIBI 51

3.2.4. Plasma cytokines in presence of DIBI treatment 57
Chapter 4: Discussion 62
4.1. Objective 1 62
4.1.1. Histology 62
4.1.2. NF-kB activation 64
4.1.3. Inflammatory mediators in plasma and lung tissue 66
4.2. Objective 2 71
4.2.1. Histology 72
4.2.2. NF-κB activation 73
4.2.3. Lung and plasma cytokine levels 75
4.3. Limitations and future directions 78
4.4. Conclusion 79
References 81
Appendices 92

LIST OF TABLES

Table 1. Characteristics of lung inflammation..... 5

Table 2. Experimental groups. 22

Table 3. Summary table for lung inflammatory mediators..... 56

Table 4. Summary table for plasma inflammatory mediators..... 61

LIST OF FIGURES

Figure 1. LPS schematic structure. 7

Figure 2. Intranasal administration of LPS. 21

Figure 3. Histopathological evaluation of lung injury post-LPS nasal instillation..... 33

Figure 4. LPS instillation increased NF-kB activation in murine lung..... 35

Figure 5. Lung levels of inflammatory mediators of LIX, CXCL2, CCL5, CXCL10, IL-1 β, IL-6, and CXCL1 were significantly increased 4 hours after LPS 5 mg/kg 39

Figure 6. Plasma levels of inflammatory mediators of CXCL2, CXCL10, IL-6, and CXCL1 were significantly increased 4 hours after LPS 5 mg/kg..... 42

Figure 7. DIBI attenuated the histopathological injury induced by LPS in mice 47

Figure 8. DIBI attenuated NF-kB activation post-LPS nasal instillation in mice 50

Figure 9. Effect of DIBI treatment on lung inflammatory mediators 55

Figure 10. Effect of DIBI treatment on plasma inflammatory mediators 60

ABSTRACT

Iron plays a critical role in the human body, e.g., in hemoglobin and DNA synthesis, but it is also important in the regulation of the immune response. Iron's role in the immune system is closely related to the catalysis of reactive oxygen species (ROS). ROS are needed to fight pathogens, but overproduction of ROS can kill healthy cells. Therefore, therapeutic iron chelation is a potential pharmacological approach to limit ROS formation and pro-inflammatory mediator release. The present research has been designed to study the impact of iron chelation by a novel, highly specific, synthetic iron chelator DIBI in an experimental model of lung inflammation in C57Bl/6 mice. First, we established a rodent lung inflammation model using intranasal instillation of LPS from *Pseudomonas aeruginosa* at different observation time points. The lung immune response was evaluated by histological analysis of lung tissue, NF-kB activation, and measurement of inflammatory cytokines and chemokines levels in plasma and lung tissues. Second, to assess the anti-inflammatory properties of DIBI, we administered DIBI intraperitoneally in the early and later stages of lung inflammation. We found that lung tissues showed significant histological injury and increased NF-κB P65 activation, 4 hours post LPS administration at a sublethal dosage (5 mg/kg). We also measured a significant elevation of LIX, CXCL2, CCL5, CXCL10, IL-1β, IL-6, and CXCL1 in the lung and CXCL2, CCL5, CXCL10, IL-6 and CXCL1 in the plasma relative to their respective control groups. Mice treated with DIBI (80 mg/kg) intraperitoneally in early stages (0 and 2 hours) after LPS-induced lung inflammation demonstrated a significant reduction of histopathological signs, reduced NF-κB P65 activation, and reduced levels of inflammatory mediators. Our data support the conclusion that LIX, CXCL2 (MIP-2), CCL5, CXCL10 (IP-10), IL-1β, IL-6, and CXCL1 (KC) play essential roles in our LPS-induced lung inflammation model. Moreover, we can conclude that DIBI administration represents a potential alternative treatment for pulmonary inflammation.

LIST OF ABBREVIATIONS USED

ALI	Acute lung injury
ARDS	Acute respiratory distress syndrome
ASL	Airway surface liquid
ATP	Adenosine triphosphate
BAL	Bronchoalveolar lavage
BCA	Bradford calorimetric assay
BSA	Bovine serum albumin
CACF	Carleton animal care facility
Casp-11	Caspase-11
CF	Cystic fibrosis
CON	Control
DCYTB	Duodenal cytochrome B
ddH2O	Double distilled H2O
DFO	Deferoxamine
DFP	Deferiprone

DFX	Deferasirox
DIBI	Denying iron from bacterial infection
DMT1	Divalent metal transporter 1
DNA	Deoxyribonucleic acid
EGFP	Enhanced green fluorescent protein
ERK 1/2	Extracellular signal-regulated kinase 1/2
FCD	Functional capillary density
FDA	Food and drug administration
FPN	Ferroprotin
H&E	Hematoxylin and eosin
HAMP	Hepcidin antimicrobial peptide
HMGB1	High mobility group box 1
i.n.	Intranasal
i.p.	Intraperitoneal
i.t.	Intratracheal
i.v.	Intravenous
ICAM-1	Intercellular adhesion molecule 1

IFN-γ	Interferon-gamma
Ig-A	Immunoglobulin-A
Ig-G	Immunoglobulin-G
IKK	IκB kinase
IL-1b	Interleukin-1 beta
IL-6	Interleukin-6
iNOS	Inducible nitric oxide synthase
Iκ-B	Inhibitory kappa B
LBP	LPS binding protein
LDH	Lactate dehydrogenase
LfR	Lactoferrin receptor
LPS	Lipopolysaccharide
MAHMP	3-hydroxy-1-(β-methacrylamidoethyl)-2-methyl-4(1 H)-pyridinone
MAPK	Mitogen activated protein kinase
MCP-1	Monocyte chemoattractant protein 1
MDA	Malondialdehyde
MPO	Myeloperoxidase

MyD88	Myeloid differentiation factor 88
NaCl	Sodium chloride
NADPH	Nicotinamide adenine dinucleotide phosphate
NETs	Neutrophil extracellular traps
NF-κB	Nuclear factor kappa B
NK cells	Natural killer cells
NLR	Nucleotide-binding oligomerization domain-like receptor
NLRP3	NOD like receptor protein 3
NS	Nova Scotia
PAMP	Pathogen-associated molecular pattern
PRR	Pattern-recognition receptor
RIPA	Radioimmunoprecipitation
ROS	Reactive oxygen species
SD	Standard deviation
TfR1	Transferrin receptor 1
Th	T helper
TLR	Toll-like receptor

TLRs	Toll like receptor
TNF-a	Tumor necrosis factor alpha
VCAM-1	Vascular cell adhesion molecule-1
VEGF-A	Vascular endothelial growth Factor

ACKNOWLEGMENTS

The last two years were the most difficult yet rewarding chapter of my life thus far, and I couldn't have done it without the help of the following people:

First, I would like to express my sincerest gratitude to my supervisors **Dr. Valerie Chappe** and **Dr. Christian Lehmann,** for their knowledge, patience, guidance, and encouragement. None of the work would have been possible without their kind help and support. Thanks to both, I learned the basic science and clinical aspects of my research. Your assistance and guidance were essential for the development of this thesis.

My primary supervisor, **Dr. Valerie Chappe**: Thank you for giving me this opportunity to work under your supervision to expand my basic science knowledge and training me to think critically to manage my project, time-wise. These skills are worth beyond the value of achieving my master's degree. You taught me skills that would assist me through my life. You were not only my mentor and supervisor but also my mother in this new country that I felt your worries and attention, especially during this chaotic year and a half, thanks to COVID-19! There is no strong word to express my gratitude.

My co-supervisor, **Dr. Christian Lehmann**: Thank you for believing in me and pushing me to my full potential. I learned a lot from you during these two years. You shaped me into the one I am now. You have always been there for me from the first day in each step of this project. Thanks for your valuable time that I know you spent revising my thesis while you were on your vacation.

Dr. Zhenyu Cheng and **Dr. Juan Zhou**: You have always been there when I needed; I appreciate your consistent help during these two years.

I also want to extend my gratitude to my other Supervisory Committee members; **Dr. Younes Anini,** and **Dr. Yassine El Hiani,** for their expertise, helpful feedback, and encouragement throughout my degree.

I am also thankful to **Dr. Orlando Hung** for accepting to be my external examiner on my thesis examining committee and providing his insightful comments and constructive feedback.

Tanya Myers and **Frederic Chappe**: for training and helping me with the histological part of the project.

Frederic Chappe and **David Allen**: for training and helping me with western blot experiments.

Bithika Ray: for training and helping me with cytokine measurements.

Dr. Audrey Li: for training me protein extraction and protein assay experiments and for providing me with insight not only for furthering my research but also for the other aspects of my life, I never forgot our delightful conversations.

Chelation Partners Inc.: for providing DIBI.

All members of the Chappe and Lehmann Labs: Dr. Anna Semaniakou, Dr. Maral Aali, Dr. Danielle Fokam, Stefan Hall, Bashir Bietar, Kayle Dickson, Cassidy Scott, Geraint Berger, Dr.

Wujood Khayat, Dr. Purvi Trivedi, and Ziba Roveimiab for helping me through my masters. I really enjoyed having been part of both these friendly and helpful teams. Special thanks to Anna, Maral, Danielle, Stefan, and Bashir, who were there for me from the beginning and during this challenging one year and a half due to COVID-19. Thank you for all the advice, but also for all the colourful moments we spent together.

My lovely family for supporting me every moment of this journey when I immigrated to Canada, especially **my parents** for their endless support and continual reassurance. I missed them so badly, and words could not describe my feelings regarding their support and love. To **Dr. Sanaz Alizadeh Tabrizi**, and **Solmaz** my dear sisters who gave me encouragement and motivation the days that research became difficult. To **Farshad**, my lovely brother-in-law, who have always been there for me no matter what and give me courage in my life. To my **uncle Bahram**, **aunt Fattaneh,** and **Sasha** who are my only family here in Canada. To **Roxana**, my dearest friend in Canada who have always been there for me in all ups and downs from the first weeks of entering to Canada. I am so lucky to have her in my life and I wish her the bests in her life. To my lovely friends, **Newsha**, **Mona, Asma**, **Sanaz, Aylar, Tara, Ali**, **Alex**, **Nikrouz**, we began as friends, and now, they are one of the dearest people to me. Finally, special thanks to **Hossein Rezaeifar**, who believed in me, kept me motivated and assisted me in every single step of these two years. He also provided me with valuable insights into various aspects of my research. I wish him a very successful PhD thesis defence soon.

Last but not least, I would like to thank all the mice sacrificed during this work and made this research feasible.

This research was supported and funded by the **Nova Scotia Graduate Scholarship** and the **Department of Physiology and Biophysics Graduate Scholarship** of Dalhousie University.

Chapter 1: Introduction

Iron is an essential nutrient for humans and nearly all animals and plants. However, dysregulation of iron homoeostasis, including iron deficiency and iron overload, can lead to serious diseases such as anemia and hemochromatosis. Recently, given the role of iron in biological processes such as in the immune system and cell proliferation, the reduction of iron bioavailability is being investigated in treating inflammatory disorders and cancer. This thesis focused on the complex role that iron plays in lung inflammation. In particular, activation of NF-κB, a transcription factor required to express several genes involved in innate immunity and inflammation, is iron-dependent (1). Therefore, this study aimed to investigate the role of novel iron chelator, DIBI, in an experimental model of rodent lung inflammation.

1.1. Lung Physiology

1.1.1. Respiratory function

The respiratory system is composed of the oro-/nasopharynx, larynx, trachea, bronchi, bronchioles, and the alveoli of the lungs. The proximity of the alveoli and the pulmonary microvasculature facilitates the exchange of oxygen and carbon dioxide. The alveolar luminal surface is mainly composed of type I alveolar cells, a thin layer of squamous epithelial cells, and type II alveolar cells which are interspersed among type I alveolar cells and produce the surfactant. Type I alveolar cells cover 90% to 95% of the alveolar surface, and its thin wall allows most of the gas exchange between the alveolar air and

the pulmonary capillary blood (2). Oxygen gets transported through the alveoli into the capillary network. It can enter the circulation and perfuse into the tissue to provide oxygen for respiration at the cellular level. Oxygen is ultimately used to produce ATP, and carbon dioxide is breathed out with other metabolic by-products (3,4). On a daily basis, a person inhales approximately 10,000 L of air. The nose and upper airway filter large particulates and warm and humidify the inspired air (5). The pulmonary epithelium functions to maintain the physiology of the respiratory system. These functions can be grouped into three categories: 1) barrier function of the epithelium; 2) the co-ordinated interaction of secretion and ciliary function, leading to adequate mucociliary clearance; and 3) secretion of substances, both derived from cells other than pulmonary epithelial cells and synthesized by pulmonary epithelial cells, which target specific environmental challenges to the pulmonary epithelial surface (3,4,6).

1.1.2. Immunological function

There is ample evidence that the lungs perform as an essential immunological organ since the pulmonary system, like other mucosal surfaces (skin and gastrointestinal tract), is in direct contact with the outside environment and continuously exposed to various microbes, organic and inorganic particulate materials (7). The innate and adaptive immune systems have developed in the respiratory tract of higher vertebrates to minimize the harmful effects of such challenges. Innate immune mechanisms in the respiratory system defend the air spaces from the nasopharynx to the alveolar membrane from the entry of microbes and microbial products into the lung. Immediate response to inhaled pathogens is an essential property of the lung innate immune system (5). Viral and bacterial particles of 1μm or smaller in size are carried to the alveolar spaces where they

interact with soluble components in alveolar fluids (e.g., IgG, complement, surfactant, and surfactant-associated proteins) and alveolar macrophages. Normally, 95% of airspace leukocytes are alveolar macrophages, 1-4 % lymphocytes, and only 1% neutrophils. Hence, alveolar macrophages are dominant phagocytic cells of innate immune system in the lungs. In general, inflammatory cells in the airways and alveolar environment can recognize the pattern recognition receptors like Toll Like Receptors (TLRs), which are founds on alveolar walls and the ciliated epithelium of the conduction airways. Airway surface fluids (ASL) in the conducting airways consist of lysozyme, lactoferrin, IgA, IgG, and defensins. Lysozyme is lytic to many bacterial membranes; lactoferrin excludes iron from bacterial metabolism; IgA, IgG, and defensins are antimicrobial peptides released from leukocytes and respiratory epithelial cells. In addition, there are high concentrations of LPS Binding Protein (LBP) and soluble CD14 (sCD14) in alveolar fluids. These molecules are the main molecules in recognition of LPS by alveolar macrophages and are explained in the next sections in detail (7,8).

Adaptive immune responses or acquired immunity induce memory responses and refer to antigen-specific immunity that often develops targeted responses following the second exposure to the specific antigen, which takes several days to mature. During adaptive immunity, pathogens encountered in the airway mucosa are transported to draining lymphoid organs where the antigen is recognized by naïve B and T lymphocytes, which causes cell activation, including T lymphocytes, cytotoxic T lymphocytes, activated macrophages, and activated Natural killer (NK) cells and the production of antibodies in response to encountered antigens and are mediated by B lymphocytes. Host cells that display foreign antigens on the cell surface, such as cells infected with viruses or

intracellular bacteria or cancer cells that express tumor antigens, are destroyed by cytotoxic T lymphocytes (often CD8+ cells) (9).

Lung tissue resident-memory T cells and memory Th1 and Th17 cells are major sources of IFN- γ and IL-17/IL-22, respectively, during recall responses and protect against infection. However, memory Th2 cells can rapidly produce IL-4, IL-5, and IL-13 in response to allergens and helminth infections (10,11).

1.2. Lung Inflammation

Acute respiratory distress syndrome (ARDS) is a clinical condition defined as acute hypoxemic respiratory failure with a non-cardiogenic cause. Although the clinical description of acute lung injury (ALI) has been defined for more than 50 years, it has undergone many changes. Based on Berlin definition of ARDS, ALI was most recently reclassified as moderate or mild ARDS (12). ARDS etiology is separated in two main categories. First, lung injury can be induced directly (locally), as in pneumonia, smoke inhalation, and aspiration, with mainly epithelial injury, or indirectly (systemically) induced by blood born insults like sepsis and pancreatitis with mainly endothelial injury (13). ARDS results in disruption of the lung endothelial and epithelial barriers inducing increased pulmonary permeability, and impairment of pulmonary gas exchange (14). Lung inflammation is characterized by clinical features, as well as physiological, biological, and pathological changes (Table 1). These responses have been suggested to be due to the increased production of inflammatory mediators, including cytokines (such as TNF-α, IL-1β, and IL-6), released mainly by neutrophils. Neutrophils appear to be one of the most important inflammatory cells involved in mechanism of lung injury since

samples of lung alveolar fluids either by bronchoalveolar lavage (BAL) or by direct aspiration of edema fluid have shown an acute neutrophilic inflammatory response (15). In addition, studies indicated that induced neutropenia followed by endotoxin challenge attenuates increases in vascular permeability and other characteristics of pulmonary damage (16).

Clinical features	• Acute onset • Diffuse bilateral alveolar injury • Acute exudative phase • Repair with fibrosis
Physiological changes	• V/Q abnormalities* • Severe hypoxemia • Decreased compliance • Impaired alveolar fluid clearance
Biological changes	• Increased endothelial and epithelial permeability • Increase in cytokine concentrations in the lungs • Protease activation • Coagulation abnormalities
Pathological changes	• Neutrophilic alveolar infiltrates • Intra-alveolar coagulation and fibrin deposition • Injury of the alveolar epithelium with denudation of the basement membrane

Table 1. Characteristics of lung inflammation. *: Ventilation/Perfusion mismatch

1.2.1. Endotoxin structure

One of the most common rodent models of lung injury is the administration of endotoxin (synonym: lipopolysaccharide, LPS). Endotoxin is a so-called pathogen-associated molecular pattern (PAMP) of the outer membrane of Gram-negative bacteria and is an extremely biologically active substance that contributes to activation and release of inflammatory mediators and serves as an early warning signal of bacterial infection (17). LPS is a biphosphorylated, polar macromolecule and is composed of three components: a

polar hydrophobic sequence of fatty acids head group (lipid A), a core glycolipid segment containing some unusual heptose and hexose moieties, and a hydrophilic oligosaccharide O antigen along its outer surface components (18,19). The antigenic specificity among species and strains of Gram-negative bacteria is duo to the variation of the polysaccharides in the O-antigen side chain. However, oligosaccharide O antigen only influences the magnitude of the inflammatory response, and most of the biological impacts of LPS are reproduced by lipid A as it retains LPS toxicity. It has been shown that Lipid A increases lung microvascular permeability leading to severe pulmonary edema with recruitment of leukocytes into the interstitial pulmonary tissue (20,21).

Studies indicated that the different timelines used for induction of experimental lung injury affect the severity of LPS-induced lung injury. As lung injury evolves over time, molecular mechanisms of pathogenesis are differentially activated during disease progression (21).

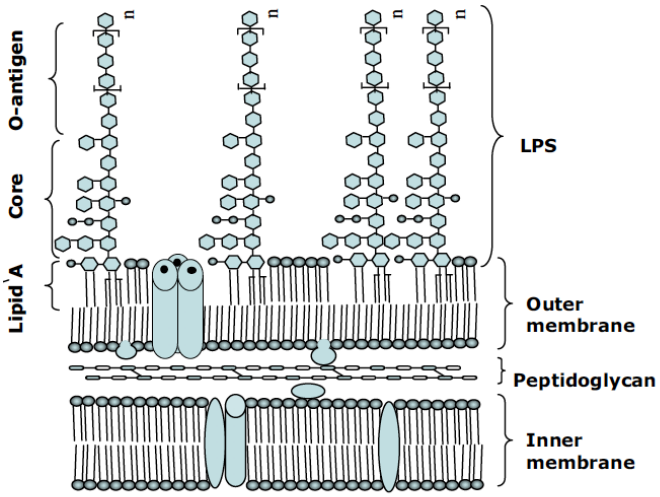

Figure 1. LPS schematic structure, adapted from "Brucella spp noncanonical LPS: structure, biosynthesis, and interaction with host immune system" by Cardoso PG, Macedo GC, Azevedo V, Oliveira SC, Microb Cell Fact. 2006;5(1):1–11(22).

1.2.2. Endotoxin response

Different pathophysiological pathways are activated during early phase of pulmonary and extra-pulmonary endotoxin challenge. Administration of LPS to the lungs through either tracheal instillation or inhalation induces direct lung injury in rodents, which damages the alveolar epithelium. Indirect lung injury is modeled by intravenous or intraperitoneal LPS administration which promotes the inflammatory mediators release into the systemic circulation, which in turn causes endothelial damage as an initial site of injury in this model (21).

The molecular response to LPS is specifically initiated after LPS binds to a specific LPS Binding Protein (LBP) and forms LPS: LBP complex. LBP performs as a shuttle

molecule to transfer LPS to CD14, which is usually attached to the cell membrane to split LPS into monomeric molecules and presents it to the TLR4–MD-2 complex and facilitate binding of LPS to its main receptor, Toll Like Receptor 4 (TLR-4), on monocytes and macrophages (18). LPS also has two other receptors in human cells: 1) CD11/CD18 molecules β2 integrins and 2) scavenger receptors for lipid molecules (23) . Once LPS binds to TLR-4, it activates Myeloid Differentiation factor 88 (MyD88), which is an intracellular adaptor protein that activates a series of signaling pathways such as the Extracellular signal-Regulated Kinase 1/2 (ERK1/2) from the mitogen activated protein kinase (MAPK) family. The activation of these MAPK signaling pathways regulates the expression of pro-inflammatory cytokines. LPS binding to TLR4, also activates the NF-κB signalling pathway (19,21). Following phosphorylation of the complex and degradation of inhibitory Iκ-B, the activated NF-κB translocates into the nucleus to promote gene regulation and the production of inflammatory cytokines (24).

NF-κB is an inactive complex of proteins present in the cytoplasm along with inhibitory proteins known as inhibitors of NF-κB, or IκBs, the most important of which is IκBα. NF-κB is composed of five structural proteins, including NF-κB1 (also named p50), NF-κB2 (also named p52), RelA (also named p65), RelB and c-Rel, which are all mediators of target gene transcription by binding to a specific DNA element, κB enhancer, as various hetero- or homo-dimers. Upon any stimulus which triggers oxidative stress (25), two major signalling pathways could activate NF-κB which is a redox-sensitive transcription factor. First, the canonical pathway which responds to different pattern recognition receptors (PRRs) and ligands of cytokines receptors and induces degradation of IκBα through phosphorylation by a multi-subunit IκB kinase (IKK) complex.

Phosphorylation of IκBs by IKK leads to rapid and transient nuclear translocation and phosphorylation of canonical NF-κB members, predominantly the p50/RelA and p50/c-Rel dimers. Second, the noncanonical or alternative pathway which does not induce phosphorylation of IκBα but induces processing of P100 involving degradation of its C-terminal IκB-like structure. This process leads to the generation of mature NF-κB2 p52 and nuclear translocation of the noncanonical NF-κB complex p52/RelB (26–28). Genes for inflammatory mediators including cytokines and chemokines have NF-κB binding site at their promoter region, and LPS exposure ultimately upregulates the synthesis of inflammatory mediators through activation of NF-κB pathway (23). The inflammasomes also play a critical role in orchestrating the initiation of inflammatory responses. Previous studies demonstrated that the nucleotide-binding oligomerization domain-like receptor (NLR) family, NOD-like receptor protein 3 (NLRP3) inflammasome augments LPS-induced ALI in mice (29). Interestingly, NF-κB signalling pathway plays a critical role in the initial steps of NLRP3 inflammasome activation (30). Recently it has been found that the key recognition molecule of intracellular LPS is caspase-11 (Casp-11). Casp-11 is activated once intracellular LPS binds to it, and then cleaved gasdermin D to mediate pyroptosis, resulting in the release of IL-1α and high mobility group box 1 (HMGB1) protein. The NLRP3 inflammasome-associated pathway to set off the release of IL-1β and IL-18 is mediated by activated Casp-11. Therefore, excessive activation of Casp-11 promotes cells pyroptosis and release of intracellular inflammatory factors (31).

1.2.3. Endotoxin types

A variety of animal models mimicking ARDS symptoms in humans are readily available to investigators. The administration of LPS is a common approach to induce lung injury

in rodents. Neutrophilic influx into the lungs of experimental animals, evidence of edema, and alveolar septal thickening are induced by intravenous and intraperitoneal injection of LPS. However, direct exposure of LPS such as intratracheal and intranasal instillation in mice can produce a controlled lung inflammation since it results in spontaneous acute self-limiting lung injury (20). Besides administration routes, LPS from different species and strains of Gram-negative bacteria induces different inflammatory responses. Stronger inflammatory responses are induced in lung tissue by LPS from *P. aeruginosa* relative to LPS from *E. coli*, which can be attributed to a different chemical structure of the O-antigen which results in different degrees of biological activity (30). The response of LPS also depends on the type of LPS that is being used. For instance, LPS from bacteria-forming smooth colonies have the O-chain, consisting of variable numbers of repeating disaccharides, and are less pyrogenic. While, LPS produced by bacteria growing in rough colonies lacks the O-chain and is prone to be more pyrogenic (17).

1.3. Iron Physiology

Iron is an essential microelement in the human body. Iron exists in two oxidation states, Fe^{2+} (ferrous) and Fe^{3+} (ferric). Due to iron's ability in facilitating electron transfer, it is an important co-factor in critical biochemical reactions including energy production (ATP synthesis) through the mitochondrial electron transport chain, as well as DNA synthesis, transcription, and repair which harbour cell proliferation and growth in both host cells and microbes. Iron is also involved in oxygen transport via hemoglobin, and last but not least in enzyme-mediated functions in immune response (33). Iron is able to

switch between the reduced and oxidized forms in the Fenton reaction and catalyses the generation of reactive oxygen species (ROS) in leukocytes. ROS are important components of the immune response to kill bacteria. However, pathologically enhanced iron levels can cause excess ROS production and promote oxidative stress. This causes cellular damage that eventually leads to cell death. Iron deficiency results in impairment of systemic oxygen delivery and cellular function (33–35).

Because of these crucial biochemical functions, and iron's propensity to produce ROS, the iron levels have to be concertedly regulated to maintain iron homeostasis in order to prevent cellular damage. Additionally, iron is not produced in the human body and there is no physiological iron excretion pathway except through shedding of mucosal and skin cells and blood loss (7-9).

1.3.1. Systemic iron homeostasis

The human body contains 3–5 g iron. Three quarter of it is present in heme associated with storage proteins including hemoglobin, found in erythroid precursors and mature erythrocytes involved in oxygen transport, and myoglobin, found in muscle fibres. Heme iron is released from aged erythrocytes (< 120 days) through phagocytosis by splenocytes and macrophages. Released heme is degraded by heme oxygenase. This iron is recovered by iron transporter proteins (ferroportin) and exported into plasma where iron is bound to transferrin. It can be reutilized in the bone marrow or is stored in hepatocytes and macrophages in the liver. The major daily source of iron (20–25 mg) in the human body is from the recycling of senescent erythrocytes (1).

Absorption of dietary iron (1–2 mg) in the form of both heme iron and non-heme iron through duodenal enterocytes is the other source of iron intake in human body. Non-heme dietary iron is in the insoluble Fe^{3+} form and is reduced to soluble Fe^{2+} form first by duodenal cytochrome b-like ferrireductase (DCYTB) which is in the apical membrane of the enterocytes. Next iron is transported across the membrane through carriers such as divalent metal transporter-1 (DMT1), a proton/divalent metal symporter, which is located at the apical membrane of the enterocytes. Nonheme iron by a common pathway together with heme-iron is either stored in tissues within iron storage proteins called ferritin (in the case of high plasma iron) and hemosiderin or transported in the circulation bound to transferrin. Ferroportin (FPN) is the only known cellular iron exporter, found in the basolateral membrane of the enterocytes (to transport absorbed iron) and in large quantities on macrophages (to transport recycled iron) and on hepatocytes (to transport stored iron). The export of iron from cells is almost exclusively managed by ferroportin, which releases iron into circulation in form of Fe^{2+}. Excreted Fe^{2+} is thereafter oxidized to Fe^{3+} by hephaestin, a homolog of ceruloplasmin, and the resulting ferric iron is bound to transferrin in the serum. It should be noted that iron is required to be bound to an iron-regulatory protein to form a stable complex. Otherwise, “free” labile iron can generate toxic radicals and damage healthy tissues and organs (7-10). The major organ for iron storage, is the liver and excess systemic iron is stored as ferritin and hemosiderin (7). Iron can also be stored at red blood cells (in hemoglobin), muscles (in myoglobin), and bone marrow (9,10).

The liver is not only the organ for iron storage, but it also regulates iron homeostasis by producing hepcidin, a circulating peptide hormone. Hepcidin binds to extracellular

domain of ferroportin and prevents its exporter activity as well as induces its internalization and degradation in enterocytes (42). Therefore, by reducing surface ferroprotin on enterocytes, hepatocytes, and macrophages, iron egress from the cells, absorption, remobilization, recycling, and generally plasma levels of iron are reduced (13–15).

Transcription of gene encoding Hepcidin Antimicrobial Peptide (HAMP), is inhibited with higher iron requirements such as by erythropoiesis. In contrast, hepcidin release is enhanced by inflammatory mediators such as interleukin 6 (IL-6) and tumor necrosis factor alpha (TNF-α), pathogenic molecules, reduced iron storage, and high plasma transferrin levels (7,9,16).

Lactoferrin also regulates unbound iron concentration and prevents ROS formation. It is a non-heme iron-binding glycoprotein which is produced by mucosal epithelial cells and granulocytes in most mammalian species. It plays an important role in defense against mucosal infections by limiting pathogen access to iron (17-19).

1.3.2. Pulmonary iron regulation

The pulmonary epithelium in the entire airway system is exposed to inhaled air containing high levels of oxygen and iron particulate matter and iron utilizing pathogens. Therefore, the bioavailability of iron in the lung must be tightly regulated to prevent iron utilization by pathogens, cytotoxicity of unbound iron, and oxidative damage. In response to these challenges, pulmonary epithelial lining fluids contain a variety of antioxidant molecules, including mucin, ascorbate, reduced glutathione as well as transferrin and lactoferrin which not only protect lungs from oxidative stress but also alter iron's redox

potential (41). The pulmonary epithelial cells also express transferrin and lactoferrin which bind to iron and can be taken up by epithelial cells and alveolar macrophages through transferrin receptor 1 (TfR1), DMT1, Zip8, and lactoferrin receptor (LfR), to be stored safely bound to ferritin inside the pulmonary epithelial cells and alveolar macrophages. Feroportin was reported to be localized on the apical layer of the human lung epithelium and also is expressed in alveolar macrophages. Additionally, hepcidin is expressed at lower levels in human airway epithelium and alveolar macrophages (11, (34).

Just as any disruptions to the above-mentioned homeostasis pathways can lead to disease, inflammation also affects iron regulation. Therefore, better understanding of the changes in iron homeostasis in the airway and the role that iron plays in the pathogenesis of lung inflammation will facilitate the utilization of iron-related pathways as target for novel anti-inflammatory therapeutic strategies.

1.4. Iron in lung inflammation

Iron plays a key role in NADPH oxidase activity, leading to ROS production which mediates inflammatory responses (49). ROS generation by phagocytic cells participates in the etiology of acute lung inflammation. Importantly, elevated iron levels through catalysis of more toxic ROS has a critical role in exacerbation of lung inflammation (34). Bronchoalveolar lavage fluid of patients with acute lung injury showed elevated concentrations of iron and iron-related proteins including ferritin, lactoferrin, and transferrin, suggesting impaired pulmonary homeostasis of iron (34,41,50). Elevated

lactoferrin prevents ROS formation and protects tissue during inflammation at the mitochondrial level (48).

Ferritin has been investigated as a predictor of acute lung injury since its levels rise as part of the inflammatory response to increase iron storage (41). Hepcidin also plays a prominent role in pulmonary inflammation through its regulation of iron transport. Expression of hepcidin is controlled by several factors including body iron stores and inflammation. Inflammatory cytokines specifically IL-6 and INF-γ induce expression of hepcidin from airway epithelial cells (41,51,52).

Studies have also demonstrated that iron influences the activation of NF-kB, a transcription factor that is required for the activation of several genes involved in innate immunity and inflammation. Elevated intracellular iron promotes the activation of NF-kB, in part by increasing ROS production, while reduced intracellular iron inhibits the phosphorylation of NF-kB that is required for its activation (1). Interestingly, it has been shown that iron directly induces TNF-α expression via NF-κB activation (53). On the other hand, enhanced TNF-α expression, for instance after LPS administration, causes intracellular iron sequestration via upregulation of the transferrin receptor and DMT1 (49).

It should be noted that cystic fibrosis (CF), one of the most frequent lethal genetic disorders among the white population, is associated with increased concentrations of iron and iron-related proteins such as ferritin, DMT1, and FPN in the lower respiratory tract. There is evidence that transferrin and lactoferrin undergo proteolysis in CF, and this may increase the amount of iron. The elevated iron levels are associated with increased levels

of inflammatory cytokines and with infectious exacerbations by *P. aeruginosa* in CF patients (41,54). TNF-α is closely related to changes in iron and ferritin content, and changes in IL-1β are related to changes in sputum ferritin content. Therefore, iron and iron-regulatory cytokines, specifically TNF-α and IL-1β, may play a role in CF lung disease (55).

1.5. Iron chelation

Iron chelators were initially designed to diminish the toxic effects of iron overload. More recently, iron chelators are being investigated as a potential treatment for other pathological conditions including local and systemic inflammation through reducing iron bioavailability for ROS production (56,57).

Three FDA approved iron chelators desferasirox (DFX), deferoxamine (DFO), and deferiprone (DFP) are currently available for treatment of iron overload diseases such as hemochromatosis, where hepcidin function is impaired, and in thalassemia, where a defect in hemoglobin production reduces erythropoiesis and frequent blood transfusions are required (58–60). DFX has been reported to show biological effects through mechanisms other than iron chelation. It prevents nuclear translocation of NF-kB and ameliorate lung inflammation through reduction of ROS generation. This reduction occurs by inhibition of NET formation through decrease in neutrophil activation and infiltration into lung tissue (61).

DIBI is a novel synthetic iron chelator developed by Chelation Partners Inc. (CPI, Halifax, NS). It has a low molecular weight (9 kDa) and is water-soluble. DIBI has a low

toxicity profile in comparison to conventional iron chelators. DIBI has a large polyvinylpyrrolidone backbone and nine 3-hydroxy-1-(βmethacrylamidoethyl)-2-methyl-4(1 H) pyridinone (MAHMP) residues. DIBI is highly selective for iron - one molecule of DIBI binds to three iron molecules (36,62). To assess toxicity of DIBI, repeated dosing of 1000 mg/kg/day (orally) and 500 mg/kg/day (intravenously), respectively, during 14 days in rats demonstrated no noticeable adverse effects and toxicity (63). To better understand the potentially beneficial effects of DIBI, this research project evaluated its potential role in pulmonary inflammation.

1.6. Hypothesis

Iron chelation by the novel iron chelator, DIBI, reduces pulmonary inflammation induced by intranasal instillation of endotoxin from *Pseudomonas aeruginosa* in mice.

1.7. Objectives

Objective 1:

Establish an experimental model of murine lung inflammation by intranasal instillation of LPS from *P. aeruginosa* using two sublethal dosages,1 mg/kg and 5 mg/kg at different time points (2 to 8 hrs post-LPS instillation) to determine the optimum dosage. Inflammation will be confirmed by histopathological changes of the lung, level of NF-κB activation and changes in lung and plasma cytokines and chemokines.

Objective 2:

Study the effects of iron chelation by the novel iron chelator DIBI on inflammatory markers of the lung response to LPS as established in Objective 1.

Chapter 2: Materials and Methods

2.1. Animals

67 Male C57BL/6 mice were purchased from Charles River Laboratories International Inc. (Saint-Constant, QC, Canada). All mice were wild type animals, 12-14 weeks old, 20-30g body weight, and housed in ventilated plastic cage racks in a pathogen free room (tested for pathogens every 3 months) of the Carleton Animal Care Facility (CACF), Faculty of Medicine, Dalhousie University, Halifax, NS, Canada. Animals were kept on a 12-hour light/dark cycle in a 21°C room and were acclimatized for 1 week in the CACF, prior to the experiments.

All experimental procedures were approved by the University Committee on Laboratory Animals at Dalhousie University under protocol number #19-010 and were performed following the guidelines and standards of the Canadian Council on Animal Care.

2.2. Experimental Model

2.2.1. Anesthesia

Animal were weighed prior to anesthesia with a commercial scale. Induction of anesthesia was accomplished by intraperitoneal (i.p.) injection of sodium pentobarbital (90 mg/kg, dilution: 54 mg/ml in normal saline, Ceva Sainte Animale, Montreal, QC, Canada) using a 25-G needle (BD PrecisionGlide^{TM}). After injection, the animal was returned to its cage on a heating pad until fully anesthetized. The pedal withdrawal reflex

(response to toe pinch) was used every 15 minutes throughout the procedure to assess the depth of anesthesia. As needed, additional doses of pentobarbital sodium (9 mg/kg; 5.4 mg/ml) were administered.

2.2.2. LPS instillation

LPS from *P. aeruginosa* was purchased from Sigma-Aldrich (Oakville, ON, Canada, L8643-10mg, source #12180104, purified by gel-filtration chromatography). LPS was diluted in sterile normal saline as suggested by the supplier (10 mg/ml stock) and stored at 4 °C. LPS was administered at a dose of 1 mg/kg or 5 mg/kg, respectively.

Anesthetized mice were placed in the palm of the handler's hand and using a pipette tip, the tongue was gently moved out and pinned down with the thumb. This ensured that the LPS solution or saline (for control animals) did not go into the stomach instead of the lungs. Small droplets of LPS or saline solution were slowly added into the left nostril of the mouse with a pipette tip (see picture below). After LPS instillation, the animal was placed back into the cage on the heating pad and monitored for the duration of the experiment (4hours, 6hours, or 8hours).

Figure 2. Intranasal administration of LPS.

2.2.3. Experimental Groups

Twelve groups of animals (n = 5-9 mice/group) were used for this study (Table 2). Lung inflammation was induced by two different LPS dosages with lung inflammation evaluated after 4, 6, and 8 hours. Treatment groups received 80 mg/kg DIBI i.p. at 0, 2, and 4 hours. DIBI (Denying Iron from Bacterial Infection) is a novel highly selective synthetic iron chelator (developed by Chelation Partners Inc., Halifax, NS), with a large polyvinylpyrrolidone backbone and nine 3- hydroxy-1-(β-methacrylamidoethyl)-2-methyl-4(1H) pyridinone (MAHMP) residues. One molecule of DIBI has affinity to bind to 3 molecules of iron (Fe^{3+}). Control animals received normal sterile normal saline.

Objective 1:

1. Control
2. LPS 1 mg/kg
3. LPS 5 mg/kg

→ Tissue collection after 4 hours

4. Control
5. LPS 1 mg/kg
6. LPS 5 mg/kg

→ Tissue collection after 8 hours

Objective 2:

7. DIBI (T=0h)
8. LPS 5 mg/kg + DIBI (T=0h)
9. LPS 5 mg/kg + DIBI (T=2h)

→ Tissue collection after 4 hours

10. Control
11. LPS 5 mg/kg
12. LPS 5 mg/kg + DIBI (T=4h)

→ Tissue collection after 6 hours

Table 2. Experimental groups.

At the end of the observation period (4, 6 or 8 hours), blood was collected by cardiac puncture. Animals were deeply anesthetized, the chest cavity was opened, and the heart was exposed. A blood sample (0.5 –0.9 ml of whole blood) was collected using a syringe connected to a 26G needle containing 20µl of sterile heparin as anti-coagulant (1000 USP units/ml, Sandoz Canada Inc.). Whole blood samples were centrifuged at 3,000 rpm for 10 minutes. Following centrifugation, plasma was collected in cryotubes and stored in a -80°C freezer until analysis. In addition, the spleen, part of small intestine (duodenum),

left lung, and brain were collected in cryotubes and flash frozen in liquid nitrogen, then transferred to -80 °C. Right lung, part of small intestine (duodenum), nasal cavity, and trachea were fixed in 10% formalin buffer for 3 days. Fixed tissues were then washed in ethanol before embedding in paraffin blocs for histological analysis.

2.3. Histology

Right lung, part of small intestine (duodenum), nasal cavity, and trachea were collected at necropsy. Tissues were fixed in 10% phosphate-buffered formalin for 3 days. Samples were then cleaned to remove all connective and muscle tissues and stored in 70% ethanol prior to embedding in paraffin blocs. Embedded tissues were then sliced into 5µm sections using a microtome and a tissue float water bath to collect section onto histology slides. Slides were dried for at least two days in an oven (56-76°C) and stored at room temperature before Hematoxylin &Eosin (H&E) staining.

H&E staining. Once the slides were dried, H&E staining was performed. First, slides were deparaffinized using sequential washes with xylene (3x), 100% ethanol (3x), 95% ethanol (2x) and 70% ethanol (2x) then put in a container with running tap water. Deparaffinized slides were then stained with filtered H&E. Slides were then washed under running tap water. Well stained slides were then dehydrated by sequential washes in 70% ethanol (2x), 95% ethanol (2x), 100% ethanol (2x) and xylene (3x). Cover slips were then mounted on slides using Cytoseal and dried overnight.

Finally, stained tissue sections were examined under light microscopy (Olympus, BH-2) and images were taken from all areas of the stained tissues.

Inflammation scoring. The degree of inflammation was then assessed and scored based on the presence of edema, hemorrhage, immune cells infiltration, cell wall thickening and the presence of aggregates. Scoring scale: 0, minimum damage; 1, mild damage; 2, moderate damage; 3, severe damage; and 4, intense damage (14).

2.4. Western blotting

2.4.1. Protein extraction for western blotting

After weighing a small sample of frozen lung tissue, every 10 mg of tissue were lysed in 50µl of radioimmunoprecipitation assay (RIPA) buffer supplemented with protease and phosphatase inhibitor cocktail using a homogenizer 985370 (120VAC, 1,2 A), on ice for 2 minutes followed by 30 seconds of vertexing. The homogenized tissue was sonicated at 30 % output for 5 cycles, followed by gentle shaking at 4 °C for 30 minutes with vertexing at 15 minutes, sonicated again at 30 % output for 3 cycles and centrifuged at 8,000 rpm for 10 minutes, at 4 °C. The supernatant was collected and following 15 minutes of gentle shaking at 4 °C, centrifuged again at 13,000 rpm for 20 minutes, at 4 °C. The second supernatant was collected, and its protein concentration was determined using Bradford assay.

2.4.2. Bradford protein assay

The Bradford protein assay was used to determine protein concentration in lung tissue lysates. A standard curve was created using Quick Start Bovine Serum Albumin (BSA) Standards (Bio-Rad, cat#5000206) at increasing concentrations of 0, 2, 5, 10, 15 µg. Protein standards were created from BSA stock (2 µg/µl) diluted in ddH2O to a final

volume of 10 µl for each concentration and added to 480 µl of ddH2O and 10 µl of RIPA (diluted to 1:4 in ddH2O). 500 µl of Quick Start Bradford 1x dye reagent (Bio-Rad, cat#5000205) was then added. 10 µl of each tissue lysates sample was first diluted in 40µl of ddH2O, then, 10µl of diluted sample was added to 490 µl ddH2O. Next, 500 µl of Bradford dye was added to each sample followed by immediate vertexing. Standards and samples were incubated at room temperature for 15 minutes before reading the ODs at 595 nm using plastic cuvettes and a Unico® 2802 UV/VIS Spectrophotometer. Duplicates of each sample and standard were measured. To obtain the standard curve, OD of standards were plotted as a function of their concentration and a linear standard curve was drawn using the protein & DNA Assay Software (Copyrights: Frederic Chappe & Valerie Chappe). To determine the protein concentration of each sample, ODs from tissue lysates of each sample was plotted against the standard curve and protein concentration for each sample was calculated according to standard curve linear regression equation.

2.4.3. SDS-PAGE electrophoresis

Tissue lysates were thawed on ice and then vortexed for a few seconds before pipetting the exact amount as calculated to obtain a total of 30µg of proteins for each sample. Sample buffer was then added to each sample and the mixture was vortexed for a few seconds. All samples were placed on a plate heater at 90 °C for 5 minutes. Once all samples were cooled down to room temperature, they were vortexed for a few seconds. 10% SDS polyacrylamide gels (10 well comb, 50µl precast gels Bio-Rad, cat#4561034) were inserted in the electrophoresis chamber containing 1L of 1x running buffer (Bio-

Rad, 10x Tris/Glycine/SDS Buffer, Cat#1610772) . Molecular weight (MW) markers and samples were loaded and run at 90 V for 30 minutes and the running was continued at 120 V until the migration line reaches the bottom of the gel. In second part, gels were transferred onto nitrocellulose membranes 0.45µm (Bio-Rad, cat#1620115) for 2 hours at 45V inside the transfer chamber containing 1L of 1x transfer buffer (Bio-Rad, 100 ml 10x Tris/Glycine Buffer, Cat#1610771, 200 ml Methanol and 700 ml ddH2O) and blotting unit and packed with ice to prevent heating of protein during the transfer. The membrane and blotting papers were pre-incubated in transfer buffer supplemented with 20% methanol for 5-10 minutes prior to the transfer. Following transfer, the membrane was saturated with 5% non-fat milk in T-TBS (Tris-buffered saline, 0.05% Tween-20) for 1 hour at room temperature with shaking and then rinsed with TBS. Primary antibody (NF-kB p65 (F-6): sc-8008 conjugated with HRP, Lot#B0520) was allowed to bind overnight at 4 °C with gentle shaking. This antibody detects both phosphorylated and non-phosphorylated P65. Next, the antibody was removed, and excess washed off with T-TBS, three times, each time 5 minutes, and at the end with TBS, one time, for 5 minutes at room temperature with shaking. Finally, the protein of interest was detected by chemiluminescence by adding 2 ml of ECL^{+} reagent mix (Bio-Rad #170-5070) with a mix solution 1:1on the membrane, allowing enzymatic reaction to continue for 5 minutes before revelation with a scanner (Bio-Rad, Chemidoc). Using ImageJ software, NF-kB protein density in each sample were estimated based on densitometry of scanned western blots. Normalization of protein of interest was performed using total protein in each sample by densitometry of scanned membrane stained with Amido black.

2.5. Lung tissue inflammatory mediators

Lung levels of selected inflammatory mediators (CCL5, CXCL2, LIX, IL-6, IL-1B, CXCL1, CXCL10, TNF-alpha, IL-17, IFN- γ) were analysed using a custom made 10-plex mouse magnetic bead-based multiplex assay obtained from R&D Bio-techne (L#139804). Bio-Plex instruments and Bio-Plex software (Bio-Rad, Mississauga, ON, Canada) were used according to protocols provided by the manufacturer. Briefly, samples were run in duplicate, and the sample dilution was 1:5 (40µl of tissue lysates mixed with 160µl of diluent) using the Bio-Plex sample diluent. Each diluted sample was added to a well of the provided microplate in the kit. Standards were prepared in two-fold serial dilutions and added to the plate along with the samples, according to the plate layout prepared. First, 50µl of detection antibody magnetic beads (microplate cocktail) were added to each well. The microplate, after securely being covered by a foil plate sealer, was incubated for 2 hours at room temperature on a horizontal orbital microplate shaker at 800 rpm and then rinsed (with wash buffer) 3 times using the Bio- Plex Pro wash station to wash away any unbound antibody. Thirdly, 50µl of diluted streptavidin-PE, which binds to the biotinylated antibody, is added to each well of microplate, securely sealed and incubated in the dark for 30 minutes, then rinsed 3 additional times to remove any unbound substrate. Next, the microplate was resuspended by adding 100µl of wash buffer with 2 minutes incubation on the shaker at 800 rpm. At this point, the formed complex is as follows: detection antibody-magnetic bead + sample + biotinylated antibodies + streptavidin-PE.

Finally, the plate was read using the Bio-Rad 200 luminometer with Bio-Plex manager software (Department of Microbiology and Immunology, Dalhousie University). Analysis with the Bio-Rad machine uses two lasers: one to excite the dyes inside each magnetic bead and identify the bead region; another one to excite the Phycoerythrin (PE) to measure the amount of analyte bound to the beads. 488 nm laser light excites PE to induce a light emission maximum of 575 nm.

Protein extraction and protein assay were required prior to the multiplex experiment to measure the amount of protein inside the tissue in each tissue sample (see below). Additionally, normalisation of each inflammatory mediators was performed after multiplex assay using the total protein content of each tissue sample (pg/ml).

2.5.1. Protein extraction for multiplex assay

Lung tissues were weighted prior to homogenization. 10 ml T-PER (Tissue Protein Extraction Reagent) buffer which enables mild extraction of total protein from tissue samples was mixed with one tablet of proteases inhibitor. 200µl of TPER supplemented with proteases inhibitor was added to each tube containing 20 mg of tissue and tissues were homogenised on ice for 2 minutes by tissue homogenizer 985370 (120VAC, 1,2 A). Next, the homogenised tissues were centrifuged at 16,000 g for 15 minutes at 4°C and then the supernatant was collected, and aliquots were stored at -80°C. Protein concentration was determined by BCA assay.

2.5.2. Protein assay for multiplex assays

Bovine Serum Albumin (BSA) was diluted in TPER buffer without the proteases inhibitor in seven increasing serial dilutions to make standards and plot the standard curve. After adding 25µl of each sample in duplicate into microplate, 200µl of BCA working reagent was added to each sample (Reagent A: B, 50:1). For 30 minutes the microplate was covered and incubated at 37 °C. Once the microplate was cooled down to room temperature, the OD was measured using microplate reader at 562 nm and protein concentration (µg/µl) was calculated based on the standard curve equation.

2.6. Plasma inflammatory mediators

The plasma multiplex assay experiment was performed with an equivalent kit from R&D Bio-techne (lot#L139804) and exactly the same method was used as for lung tissue samples except that the sample dilution was 1:2 (50µl of plasma mixed with 50µl of diluent), and there was no need for protein extraction, protein assay prior to the multiplex experiment and for normalisation of each inflammatory mediators after multiplex assay.

2.7. Statistical analysis

All data were analysed using the software Prism 9 version 9.1.2 (225) (GraphPad Software, La Jolla, CA, USA). To confirm normal distribution of data, the Kolmogorov-Smirnov Test was used. Pairwise comparisons were performed using Student's t-test. One-way ANOVA followed by Tukey's multiple comparison test was used to analyze normally distributed data for 3 or more groups. Data was expressed as mean ± standard deviation (SD). Significance was assumed at P values less than 0.05 ($P<0.05$).

Chapter 3: Results

The murine lung immune response to bacterial toxins and to DIBI treatment post LPS instillation were evaluated by histological analysis of lung tissue using H&E staining, NF-kB activation, and measurement of inflammatory cytokines and chemokines levels in plasma and lung tissue.

3.1. Objective 1: Establish murine lung inflammatory model by intranasal instillation of LPS

We first established the dosage and time frame for LPS from *Pseudomonas aeruginosa* to induce significant increase in histopathological injury of the murine lung tissue and the level of inflammatory mediators in lung tissue and plasma.

3.1.1. Histology

Histopathological changes in lung tissue were evaluated by H&E staining after intranasal administration of LPS from *pseudomonas aeruginosa* or Saline buffer as control.

The control group (CON) which received Saline (0.9% NaCl) only, presented minimal to no inflammation and damage (histopathological score = 0.64+0.27) based on the scoring method which is described in the method section.

Histological examination of lung tissues from the LPS groups showed significant changes including oedema, alveolar haemorrhage, pro-inflammatory cells infiltration, and thickening of the alveolar wall 4 hours after LPS instillation at a dosage of 5 mg/kg

(2.51+0.20) when compared to control group (Fig. 1). Those receiving 1 mg/kg LPS also showed significant histopathological injury after 4 hours in terms of thickening of the alveolar wall and pro-inflammatory cells infiltration relative to control group (1.67+0.43). There was more inflammatory alteration in lung tissue 4 hours after instillation of LPS at 5 mg/kg relative to 8 hours timepoint with similar dosage (1.78+0.26). Moreover, 8 hours after instillation of 1 mg/kg and 5 mg/kg LPS, histopathological changes were not statistically significant in comparison to control group at 8h timepoint (CON8h). CON8h also indicated some level of lung injury but it was not significantly different from CON4h.

These results indicated that significant histopathological changes in lung tissue can be obtain 4 hours after intranasal administration of 5 mg/kg dosage of LPS. This tissue inflammation seemed to have spontaneously resolved 8 hours after LPS instillation.

A

Control after 4 h

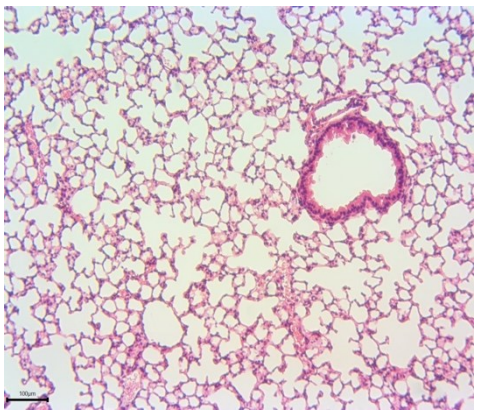

LPS 1 mg/kg after 4 h

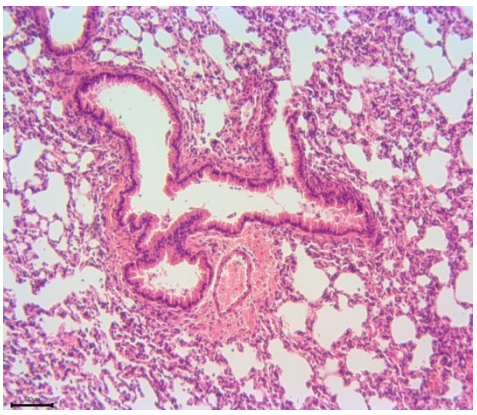

LPS 5 mg/kg after 4 h

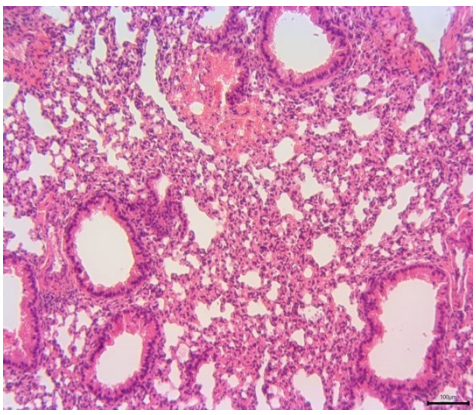

Control after 8 h

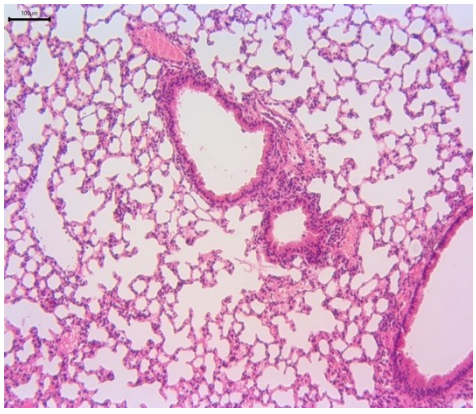

LPS 1 mg/kg after 8 h

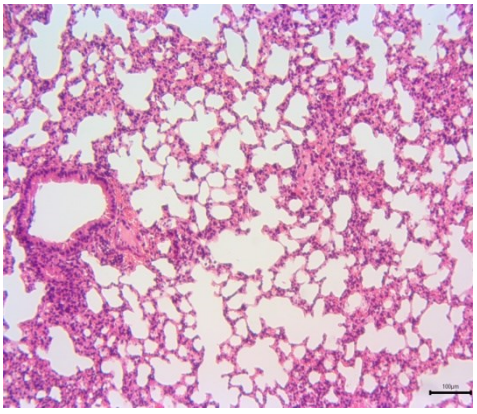

LPS 5 mg/kg after 8 h

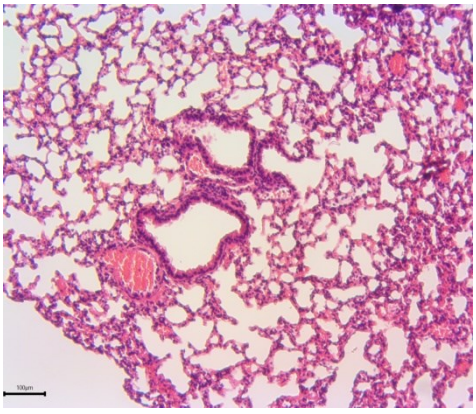

B

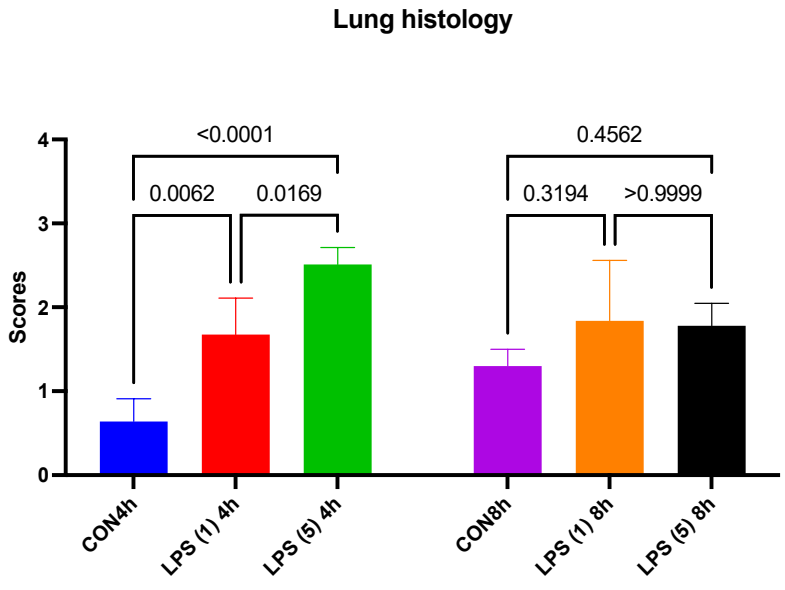

Figure 3. Histopathological evaluation of lung injury post-LPS nasal instillation. C57BL/6 mice received LPS (1 or 5 mg/kg, i.n.) or 0.9% NaCl (Saline) for 4 and 8 hours as indicated. Histopathological changes in H&E-stained lung tissue sections were observed using light microscopy (100x magnification). A, Representative images of H&E-stained lung tissue sections. Scale bar represents 100 µm. B, Lung injury scores (0-4) were used to semi-quantify histopathological injuries observed in tissue sections (see the Method section for details). Data were expressed as means ± SD of 10 images per lung (n = 5-9 mice per group), p values are indicated on top of each comparison bars. CON4h: control after 4 hours Saline, LPS (1) 4h: 1 mg/kg of LPS after 4 hours, LPS (5) 4h: 5 mg/kg of LPS after 4 hours, CON8h: control after 8 hours of saline, LPS (1) 8h: 1 mg/kg LPS after 8 hours, LPS (5) 8h: 5 mg/kg LPS after 8 hours.

3.1.2. NF-κB activation by LPS

Flash frozen lung tissues were used in immunoblotting experiments to study NF-κB activation. Since the antibody which was used in this study detected both the phosphorylated and non-phosphorylated p65, we could measure the increase in signal upon activation of NF-κB. The results of western blot experiments showed that NF-κB activation was significant in the lung of mice 4 hours after receiving 5 mg/kg LPS in comparison to the control group (Figure 2, $p < 0.0001$).

However, NF-κB activation was significantly reduced ($p < 0.0001$) 8 hours after LPS (5 mg/kg) instillation in comparison to the 4 hours group and no significant changes were found relative to its control group (CON8h) where some level of NF-κB activation was found.

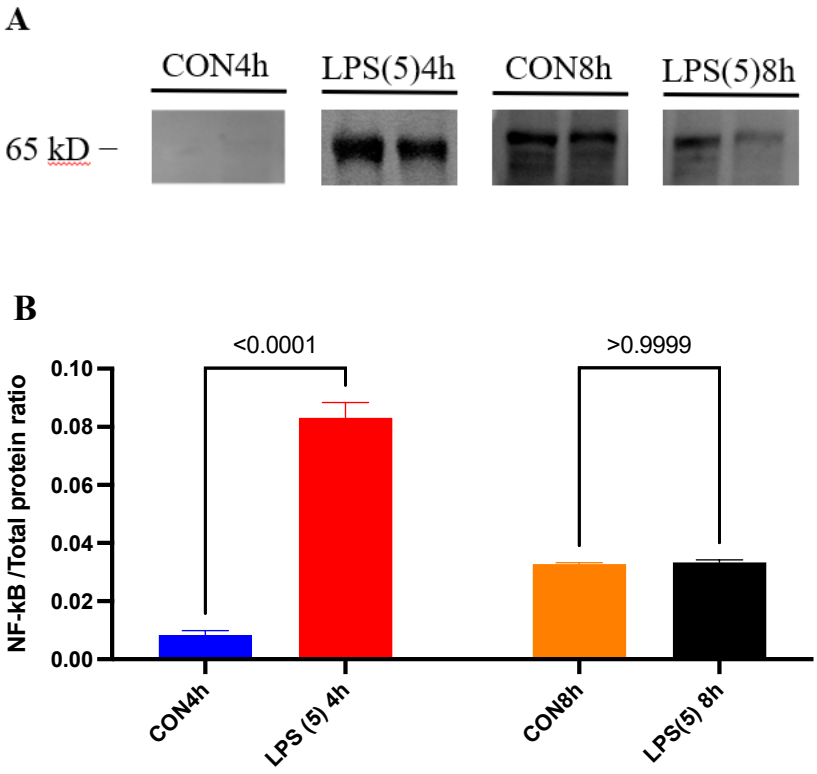

Figure 4. LPS instillation increased NF-κB activation in murine lung. Phosphorylated NF-κB (65kD) was detected using western blotting with a specific anti-p65NF-κB antibody. A, Representative western blot images. B, Semi-quantification of NF-κB signal. Data were expressed as means ± SD for each group (n = 5-9 mice per group), p values are indicated on top of each comparison bars. CON4h: control after 4 hours, LPS (5) 4h: LPS 5 mg/kg after 4 hours, CON8h: control after 8 hours, and LPS (5) 8h: LPS 5mg/kg after 8 hours.

3.1.3. Lung cytokines

To confirm if any other inflammatory mediators than NF-κB are involved in the inflammatory response of lung tissue to *Pseudomonas aeruginosa* LPS instillation, the level of cytokines and chemokines in lung tissue were measured by multiplex assay.

Four hours after administering 5mg/kg of LPS, a significant increase of LIX, CXCL2, CCL5, CXCL10, IL-1β, IL-6, and CXCL1 levels were measured relative to control tissues (CON4h) and relative to the instillation of 1 mg/kg LPS (Figure 3A to G). Additionally, 1 mg/kg LPS after 4 hours induced significant increase only in LIX and CCL5 levels relative to control group (CON4h, Figure 3A & C).

Both dosages of 1 mg/kg and 5 mg/kg LPS caused significant increase in lung level of CXCL1 after 8 hours relative to control group (CON8h, Figure 3G). While after 8 hours, only 1 mg/kg dosage of LPS induced a significant increase in the lung level of CXCL10 relative to control group (CON8h, Figure 3D).

TNFα was undetectable in lung tissue extracts from the control groups (CON4h and CON8h). TNFα was also not significantly increased after 4 hours in groups receiving 5mg/kg of LPS relative to 1 mg/kg LPS. Both LPS dosages of 1 mg/kg and 5 mg/kg LPS after 8 hours, induced low levels of TNFα and were not significantly different (data not shown).

In this study, IL-17 and IFN-γ were not detected in any of the treatment group tested (not shown here).

DIBI treatment alone, injected intraperitoneally at a dosage of 80mg/kg did not induce any change in all the cytokines measured in lung tissue extracts after 4 hours.

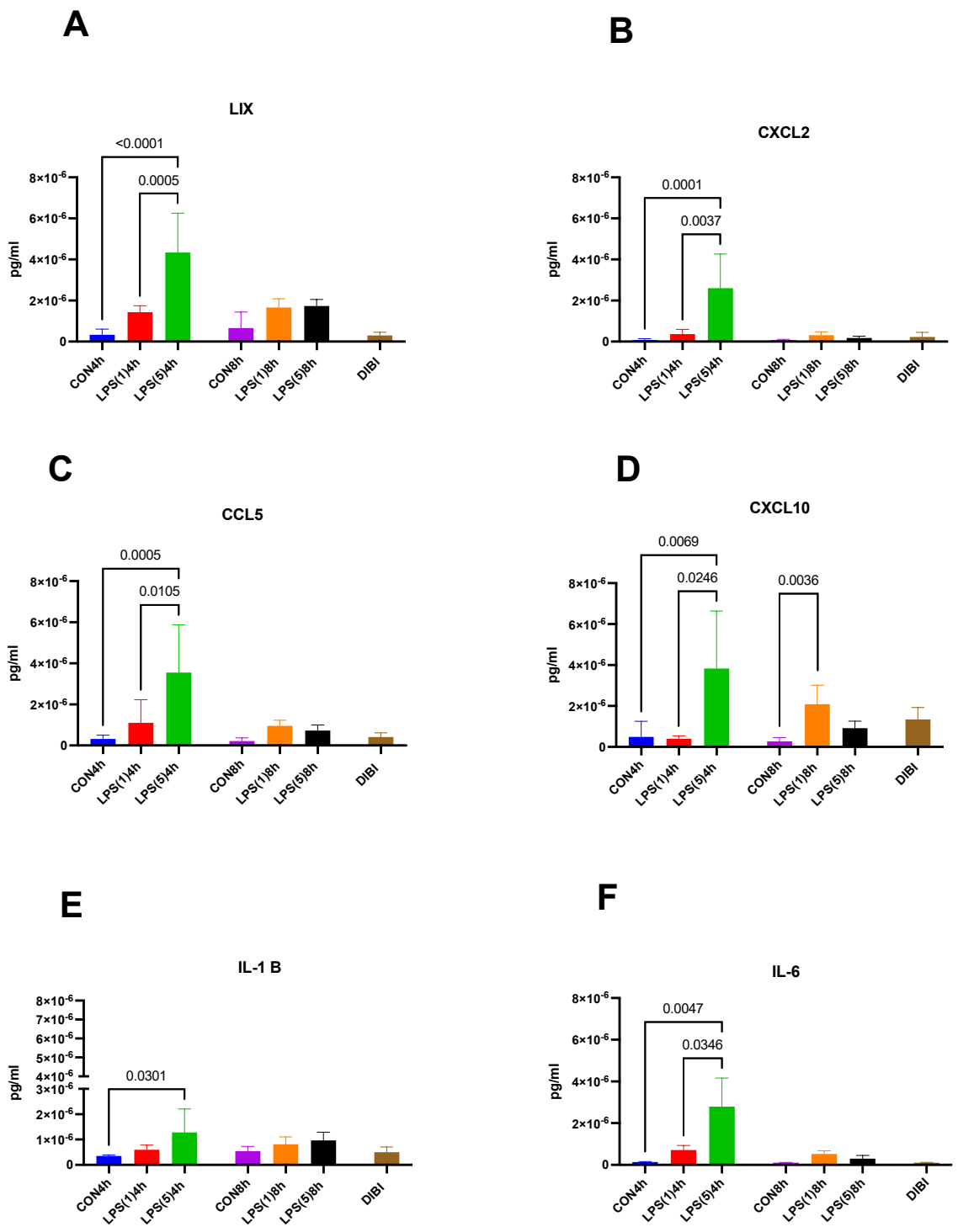
A
LIX
<0.0001
0.0005
pg/ml
8×10-6
6×10-6
4×10-6
2×10-6
0
CON4h
LPS(1)4h
LPS(5)4h
CON8h
LPS(1)8h
LPS(5)8h
DIBI
B
CXCL2
0.0001
0.0037
C
CCL5
0.0005
0.0105
D
CXCL10
0.0069
0.0246
0.0036
E
IL-1 B
0.0301
7×10-6
5×10-6
3×10-6
1×10-6
F
IL-6
0.0047
0.0346

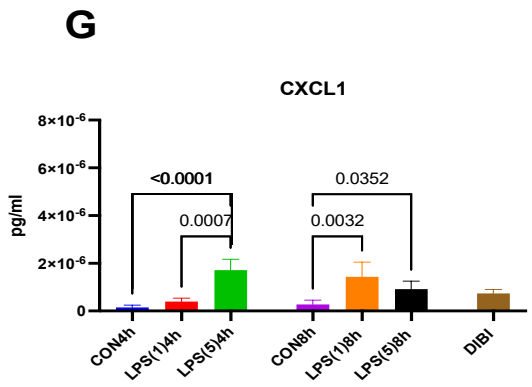

Figure 5. Lung levels of inflammatory mediators of LIX, CXCL2, CCL5, CXCL10, IL-1 β, IL-6, and CXCL1 were significantly increased 4 hours after LPS 5 mg/kg. Levels of inflammatory mediators as indicated were measured by Luminex assays on lung tissues extracts from mice treated with LPS at 1 mg/kg and 5 mg/kg, respectively after 4 and 8 hours and 4 hours after administration of DIBI at a dosage of 80 mg/kg. Histograms represent Means ± SD values from n=5-9, p values for significant differences are indicated on top of each comparison bars. CON4h: Control after 4 hours, LPS(1) 4 h: LPS 1 mg/kg after 4 hours, LPS(5) 4 h: LPS 5 mg/kg after 4 hours, CON8h: Control after 8 hours, LPS(1) 8h: LPS 1mg/kg after 8 hours, LPS(5) 8 h: LPS 5 mg/kg after 8 hours.

3.1.4. Plasma cytokines

Cytokines present in the plasma collected at necropsy for each mouse in all groups tested were then measured in multiplex assays as before.

Four hours after administering 5mg/kg of LPS, significant increase in plasma levels of CXCL2, CCL5, CXCL10, and IL-6, and CXCL1 were measured relative to control group (CON4h, Figure 4 B, C, D, E, and G). However, four hours after receiving 1 mg/kg LPS no significant changes were observed in the plasma level of the mentioned inflammatory mediators relative to control group (CON4h, Figure 4A-G).

Both dosages of 1 mg/kg and 5 mg/kg LPS after 8 hours, did not cause significant increase in LIX, CXCL2, CXCL10, IL-6, and IL-17, and CXCL1 levels in plasma relative to control group (CON8h, Figure 4 A, B, D, E, F, and G). However, eight hours after instillation of 5 mg/kg LPS, CCL5 level in plasma was significantly increased in comparison to after the four hours timepoint ($p<0.0001$, Figure 4 C). 1 mg/kg dosage of LPS did not induce significant increase in plasma level of CCL5 relative to control group (CON8h, Figure 4 C).

Control level of TNF-α was undetectable after 4 hours. Eight hours after administration of 5 mg/kg LPS, plasma level of TNF-α increased, but was undetectable in the LPS 1 mg/kg treatment group.

IL-1 Beta and IFN-γ were undetectable in our assay, for all tested samples.

Cytokines and chemokines levels with DIBI at a dosage of 80mg/kg were variable and none of them showed significant difference with Control (Figure 4 A-G).

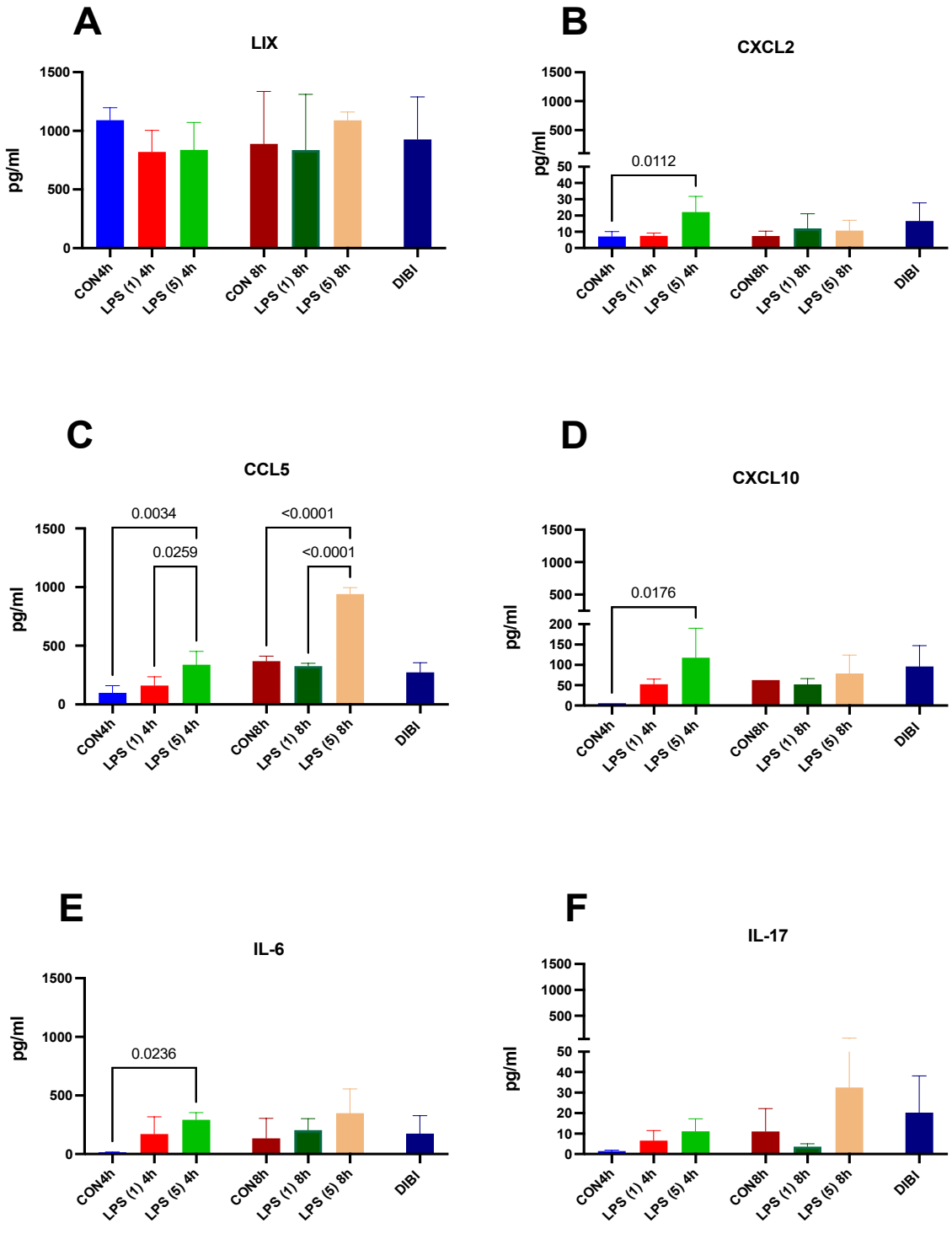
A
LIX
pg/ml
1500
1000
500
0
CON4h
LPS (1) 4h
LPS (5) 4h
CON 8h
LPS (1) 8h
LPS (5) 8h
DIBI
B
CXCL2
pg/ml
0.0112
C
CCL5
0.0034
0.0259
<0.0001
<0.0001
D
CXCL10
0.0176
E
IL-6
0.0236
F
IL-17

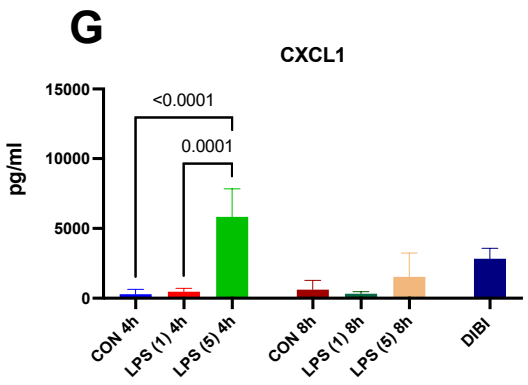

Figure 6. Plasma levels of inflammatory mediators of CXCL2, CCL5, CXCL10, IL-6, and CXCL1 were significantly increased 4 hours after LPS 5 mg/kg. Data were expressed as means ± SD (n = 5-9 mice per group), and p values are indicated on top of each comparison bars.CON4h: Control after 4 hours, LPS (1) 4 h: LPS 1 mg/kg after 4 hours, LPS (5) 4 h: LPS 5 mg/kg after 4 hours, CON8h: Control after 8 hours, LPS (1) 8h: LPS 1mg/kg after 8 hours, LPS (5) 8 h: LPS 5 mg/kg after 8 hours, and DIBI: DIBI 80 mg/kg after 4 hours.

3.2. Objective 2: Study the effects of iron chelation by DIBI on the inflammatory markers of lung inflammation established in Objective 1

In a second objective we evaluated the anti-inflammatory effect of DIBI as a novel iron chelator at dosage of 80 mg/kg at different time point post administration of 5 mg/kg LPS from *Pseudomonas aeruginosa* intranasally. We scored histopathological injury inside the murine lung tissue and measured the level of inflammatory mediators in plasma and lung tissue.

3.2.1. Histology

Histopathological changes in LPS-inflamed lung tissues after treatment with the iron chelator DIBI were evaluated by H&E staining. Administration of LPS (5 mg/kg, intranasal instillation) resulted in significant lung injury including oedema, alveolar haemorrhage, proinflammatory cells infiltration, and thickening of the alveolar wall, 4 hours (2.51+0.20) and 6 hours (2.02+0.69) after instillation in comparison to their respective control groups (CON4h and CON6h, Figure 5).

Intraperitonially injection of DIBI at dosage of 80 mg/kg did not induce significant lung injury in terms of above-mentioned parameters after 4 hours relative to control group (CON4h). In addition, intraperitonially injection of DIBI at dosage of 80 mg/kg at time 0 and 2 hours after LPS instillation, significantly attenuated histopathological changes induced by LPS, (Figure 5A & C). However, administration of DIBI, 4 hours after LPS

instillation could not reduce the inflammation significantly in comparison to LPS treatment alone (LPS after 6 hours), (Figure 5B & D).

These results indicated that DIBI attenuated histopathological injury induced by LPS, in the early treatments (0 h and 2 hours after LPS instillation).

A

CON4h

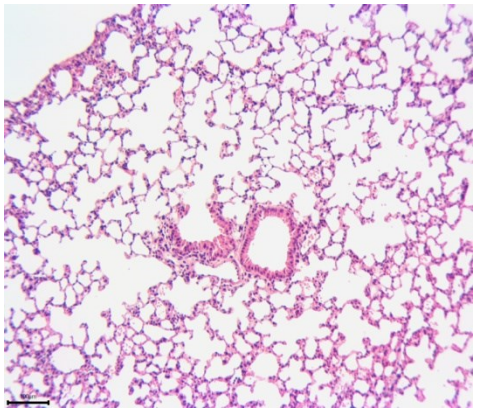

LPS (5) 4h

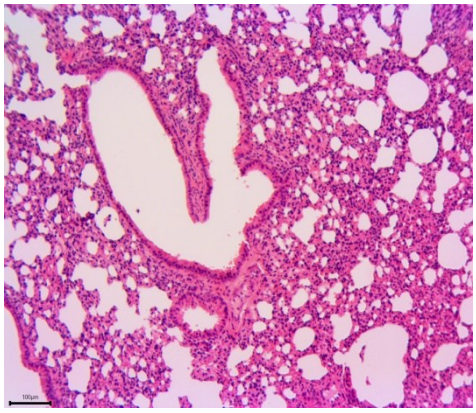

LPS (5)4 h+ DIBI(@0h)

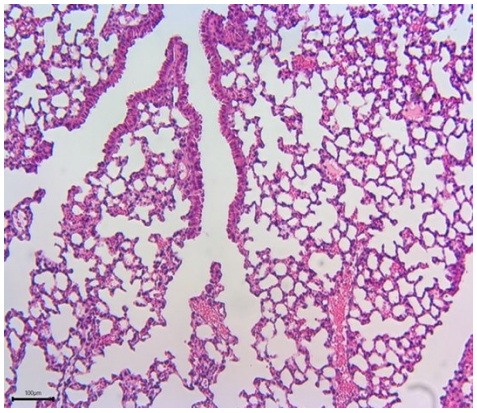

LPS (5)4 h+ DIBI(@2h)

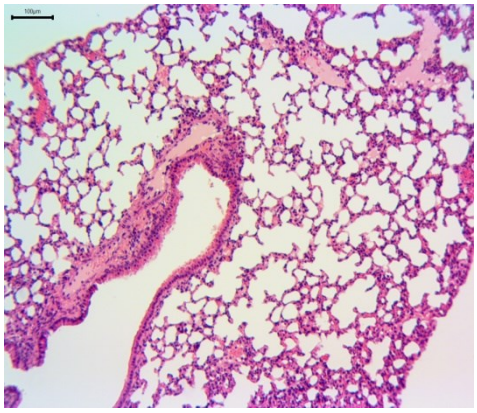

B

CON6h

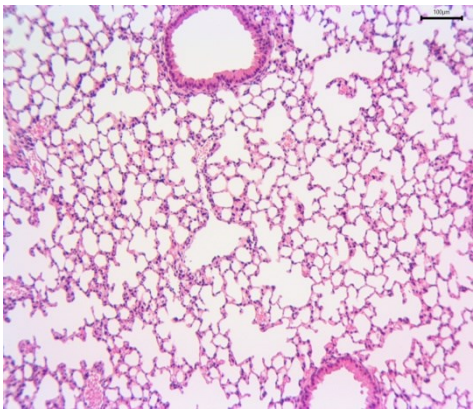

LPS (5) 6h

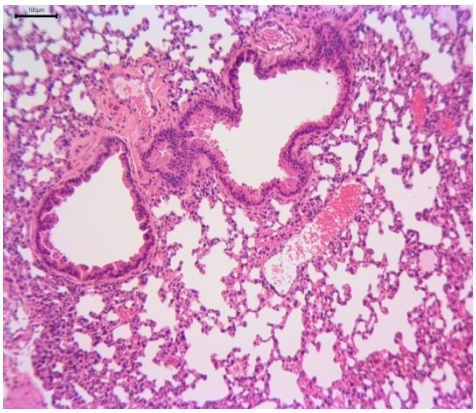

LPS (5)6 h+ DIBI(@4h)

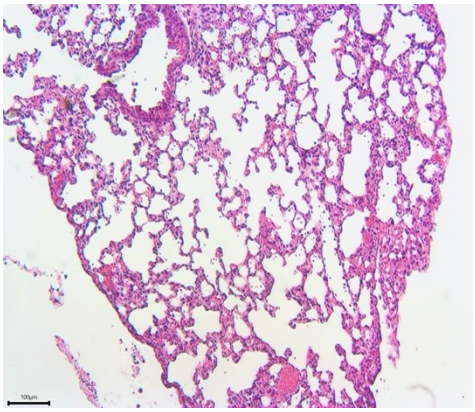

DIBI

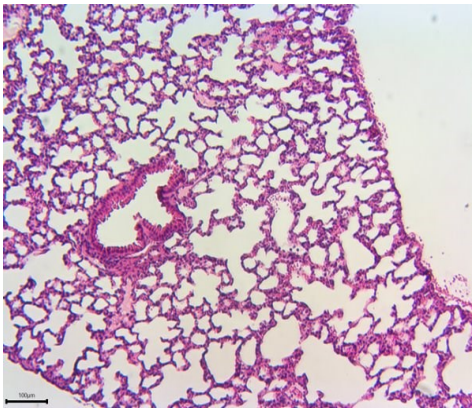

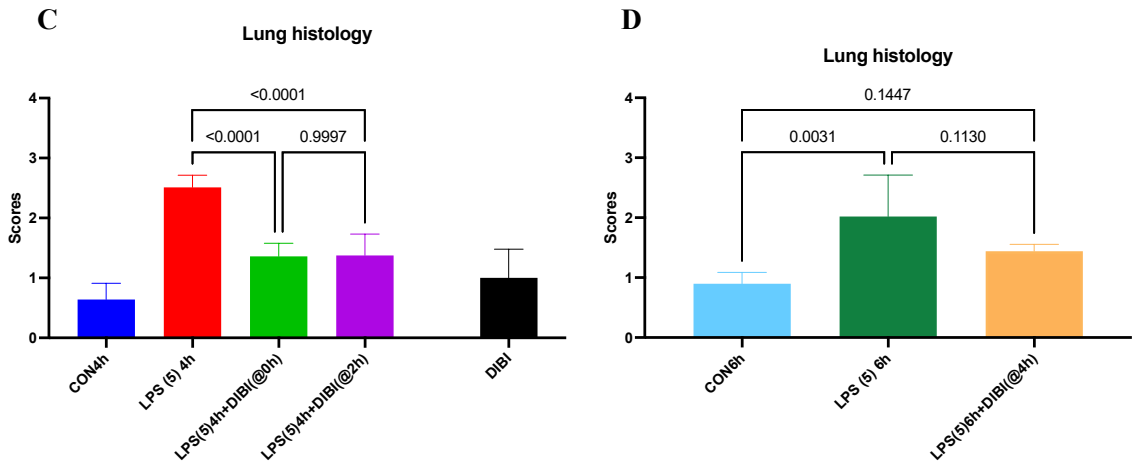

Figure 7. DIBI attenuated the histopathological injury induced by LPS in mice. C57BL/6 mice received LPS administration (5 mg/kg, i.n.). Histopathological changes were observed using light microscopy of H&E-stained lung tissue sections (100x magnification), 4 hours (A) and 6 hours (B) after LPS instillation with or without DIBI treatment as indicated. Scale bar represents 100 μm. C & D, Lung injury scores (0-4) were used to semi-quantitatively evaluate the histopathological injury determined on H&E pictures. Data are expressed as means ± SD for 10 images per lung (n = 5-9 mice per group), and p values are indicated on top of each comparison bars. CON4h: Control group after 4 hours Saline, LPS (5) 4h: LPS 5mg/kg after 4 hours group, LPS(5)4h+DIBI(@0h): LPS 5mg/kg after 4 hours and DIBI administration at time 0hour post LPS instillation, LPS(5)4h+DIBI(@2h): LPS 5mg/kg after 4 hours and DIBI administration at time 2 hours post LPS instillation, and DIBI: 4 hours after administration of DIBI at dosage of 80 mg/kg. CON6h: Control group after 6 hours Saline, LPS (5) 6h: LPS 5mg/kg after 6 hours group, LPS(5)6h+DIBI(@4h): LPS 5mg/kg after 6 hours and DIBI administration at time 4 hours post LPS instillation.

3.2.2. NF-κB activation by LPS and effect of DIBI treatment

Early treatment with the iron chelator DIBI at dosage of 80 mg/kg, 0 and 2 hours after LPS instillation significantly reduced NF-κB activation in the lung tissue in comparison to the LPS 5 mg/kg after 4 hours group (Figure 6, $p<0.0001$).

While 6 hours after intranasal instillation of LPS 5 mg/kg a significant increase in NF-κB activation was observed in comparison to control group (Figure 6), DIBI administration 4 hours after LPS instillation still significantly reduced NF-κB activation in comparison to LPS alone (Figure 6B, $p<0.0001$).

These data indicate that reduction of NF-κB activation contributed to the protective effect of DIBI against LPS-induced lung inflammation in mice.

A

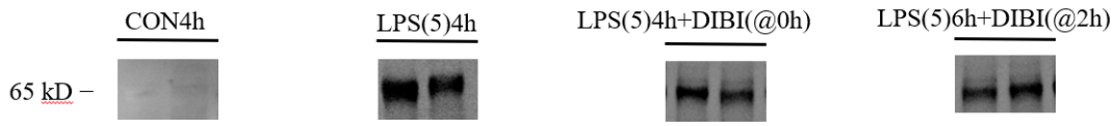
CON4h
LPS(5)4h
LPS(5)4h+DIBI(@0h)
LPS(5)6h+DIBI(@2h)
65 kD –

B

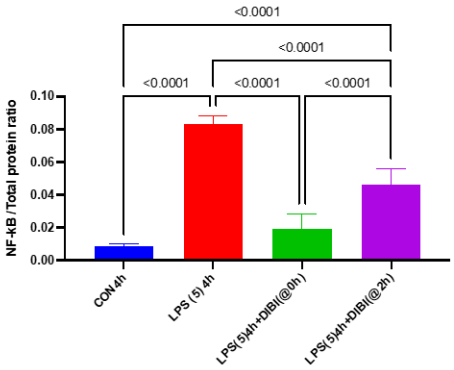
<0.0001
<0.0001
<0.0001
<0.0001
<0.0001
NF-kB /Total protein ratio
0.10
0.08
0.06
0.04
0.02
0.00
CON4h
LPS (5) 4h
LPS(5)4h+DIBI(@0h)
LPS(5)4h+DIBI(@2h)

C

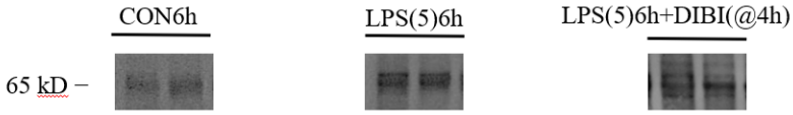
CON6h
LPS(5)6h
LPS(5)6h+DIBI(@4h)
65 kD –

D

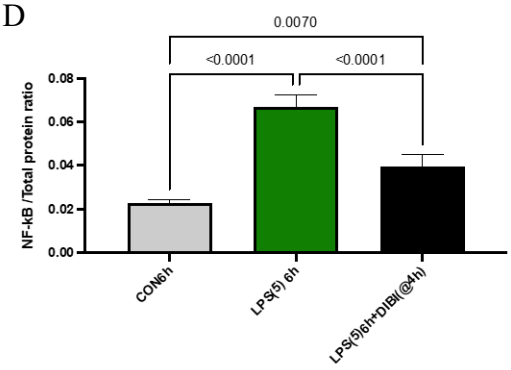
0.0070
<0.0001
<0.0001
NF-kB /Total protein ratio
0.08
0.06
0.04
0.02
0.00
CON6h
LPS(5) 6h
LPS(5)6h+DIBI(@4h)

Figure 8. DIBI attenuated NF-κB activation post-LPS nasal instillation in mice. Phosphorylated NF-kB was detected using western blotting with a specific anti-p65NF-κB antibody. A & C, Representative western blot images. B& D, Semi-quantification of NF-κB signal. Data were expressed as means ± SD for each group (n = 5-9 mice per group), p values for significant differences are indicated on top of each comparison bars. CON4h: Control group after 4 hours Saline, LPS (5) 4h: LPS 5mg/kg after 4 hours group, LPS(5)4h+DIBI(@0h): LPS 5mg/kg after 4 hours and DIBI administration at time 0 hour post LPS instillation, LPS(5)4h+DIBI(@2h): LPS 5mg/kg after 4 hours and DIBI administration at time 2 hours post LPS instillation, CON6h: Control group after 6 hours Saline, LPS (5) 6h: LPS 5mg/kg after 6 hours group, LPS(5)6h+DIBI(@4h): LPS 5mg/kg after 6 hours and DIBI administration at time 4 hours post LPS instillation.

3.2.3. Lung cytokine levels in presence of DIBI

There was a significant increase in LIX, CXCL2, CCL5, and CXCL10, IL-1β, IL-6, and CXCL1 levels in lung tissues 4 hours after the administration of LPS at 5mg/kg relative to control group (CON 4 h, Figure7A-G). However, administration of DIBI with a dosage of 80 mg/kg at time 0 hour after LPS instillation and at time 2 hours post LPS instillation significantly reduced the levels of LIX, CXCL-2, CCL5, and IL-6 in lung tissue relative to LPS 5 mg/kg. No remarkable difference between early treatment with DIBI at time 0 and 2 hours post-LPS was observed in LIX, CXCL-2, CCL5, and IL-6 lung levels.

While lung levels of LIX, CXCL2, CCL5, and CXCL10, IL-1β, IL-6, and CXCL1 were significantly increased 6 hours after LPS instillation in comparison to control group (CON6h), DIBI administration at time 4 hours after LPS instillation could significantly reduce the level of CXCL-2, CCL5, and IL-6 in lung tissues, but not to the control levels.

CXCL10, and IL-1B, and CXCL1 levels after DIBI treatment at all time point (0, 2, and 4 hours after LPS instillation) were not significantly different from LPS treatment groups (LPS (5)4h and LPS(5)6h).

Control level of TNF-α after 4 hours was undetectable in our assay. Four hours after administering 5mg/kg of LPS, lung level of TNF-α was increased. The level of TNF-α for control after 6 hours (CON6h), LPS 5mg/kg after 6 hours and DIBI treatment was undetectable (Data not shown).

IL-17 and IFN-γ levels in the lung were undetectable for all treatment groups tested.

The changes in levels of studied inflammatory mediators in the lung tissue were summarized in Table 3.

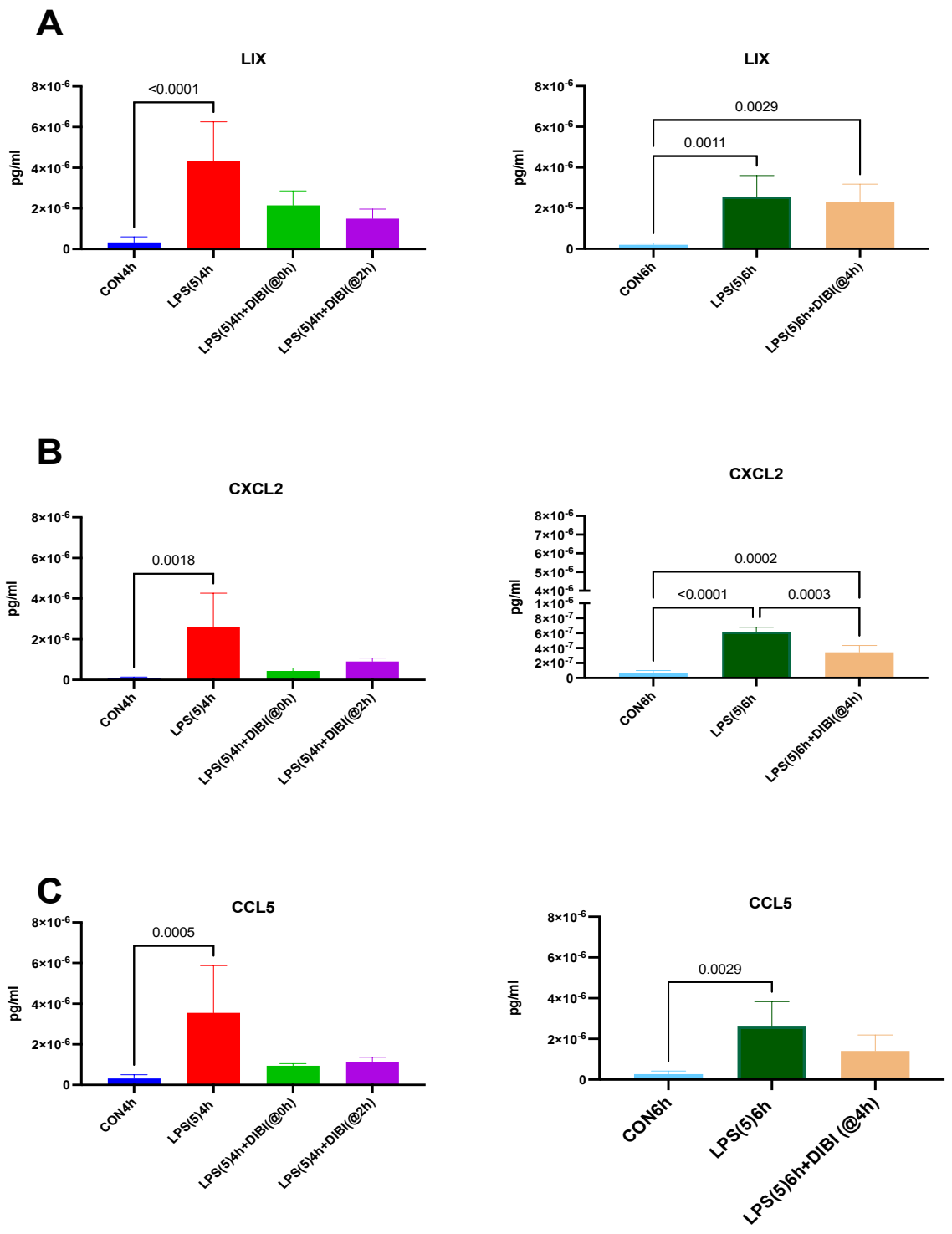
A
LIX
pg/ml
<0.0001
CON4h
LPS(5)4h
LPS(5)4h+DIBI(@0h)
LPS(5)4h+DIBI(@2h)
LIX
0.0029
0.0011
CON6h
LPS(5)6h
LPS(5)6h+DIBI(@4h)
B
CXCL2
0.0018
0.0002
<0.0001
0.0003
C
CCL5
0.0005
0.0029
LPS(5)6h+DIBI (@4h)

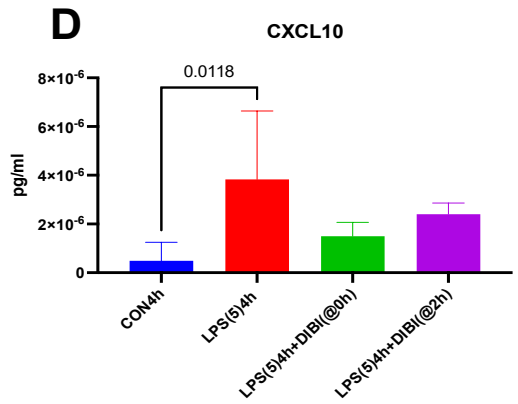
D
CXCL10
0.0118
pg/ml
8×10-6
6×10-6
4×10-6
2×10-6
0
CON4h
LPS(5)4h
LPS(5)4h+DIBI(@0h)
LPS(5)4h+DIBI(@2h)

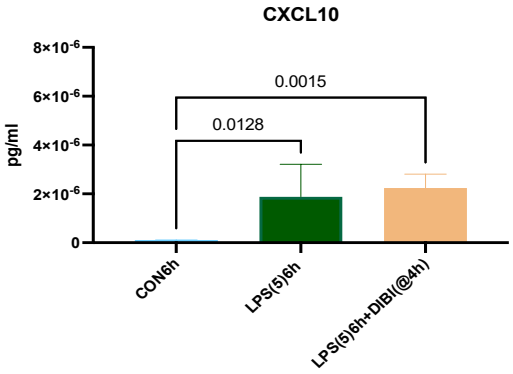
CXCL10
0.0015
0.0128
pg/ml
8×10-6
6×10-6
4×10-6
2×10-6
0
CON6h
LPS(5)6h
LPS(5)6h+DIBI(@4h)

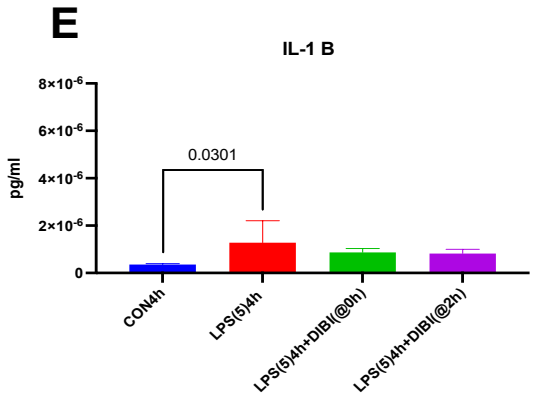
E
IL-1 B
0.0301
pg/ml
8×10-6
6×10-6
4×10-6
2×10-6
0
CON4h
LPS(5)4h
LPS(5)4h+DIBI(@0h)
LPS(5)4h+DIBI(@2h)

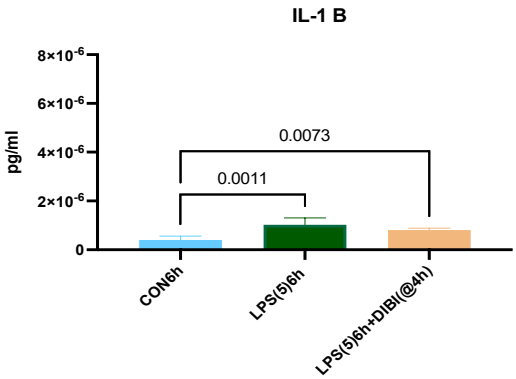
IL-1 B
0.0073
0.0011
pg/ml
8×10-6
6×10-6
4×10-6
2×10-6
0
CON6h
LPS(5)6h
LPS(5)6h+DIBI(@4h)

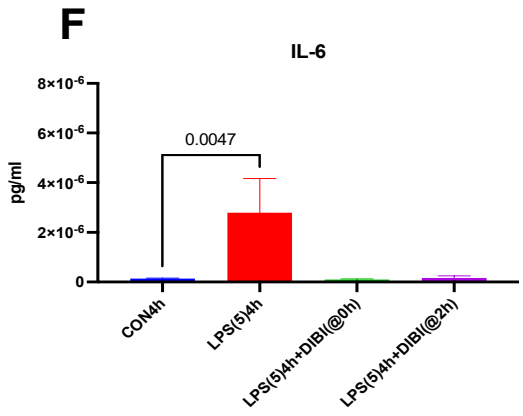
F
IL-6
0.0047
pg/ml
8×10-6
6×10-6
4×10-6
2×10-6
0
CON4h
LPS(5)4h
LPS(5)4h+DIBI(@0h)
LPS(5)4h+DIBI(@2h)

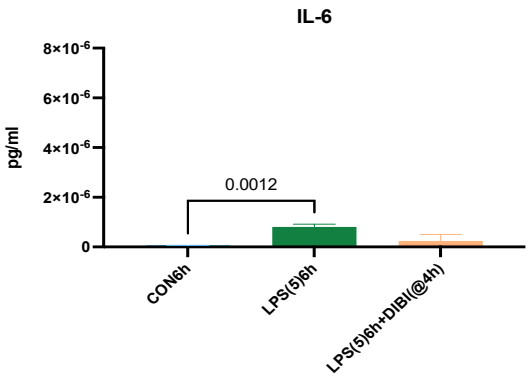
IL-6
0.0012
pg/ml
8×10-6
6×10-6
4×10-6
2×10-6
0
CON6h
LPS(5)6h
LPS(5)6h+DIBI(@4h)

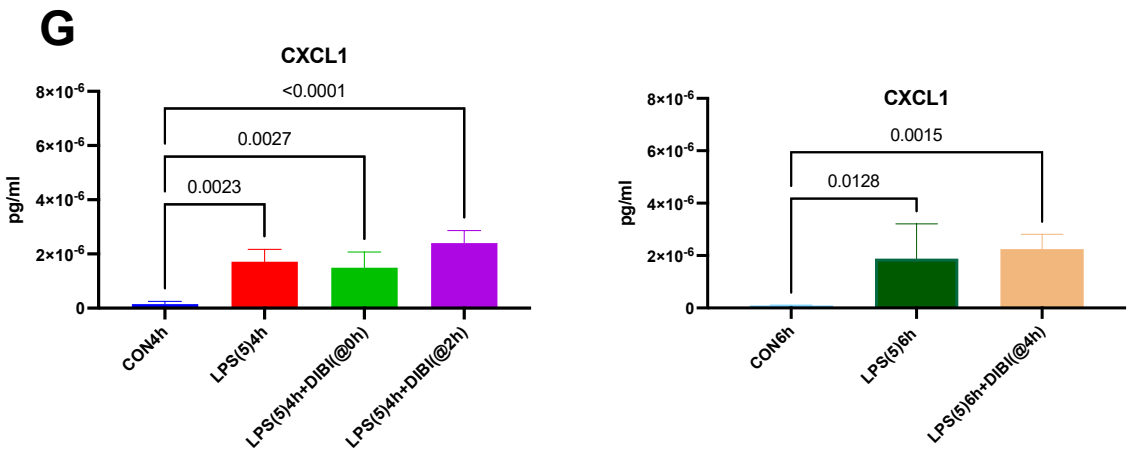

Figure 9. Effect of DIBI treatment on lung inflammatory mediators. Early DIBI treatment at dosage of 80 mg/kg at 0 hour and 2 hours post-LPS instillation significantly reduced the levels of inflammatory mediators, but not when administered 4 hours post LPS installation (5 mg/kg). Data were expressed as means ± SD for each group (n = 5-9 mice per group), and p values are indicated on top of each comparison bars. CON4h: Control group after 4 hours Saline, LPS (5) 4h: LPS 5mg/kg after 4 hours group, LPS(5)4h+DIBI(@0h): LPS 5mg/kg after 4 hours and DIBI administration at time 0 hour post LPS instillation, LPS(5)4h+DIBI(@2h): LPS 5mg/kg after 4 hours and DIBI administration at time 2hours post LPS instillation, CON6h: Control group after 6 hours Saline, LPS (5) 6h: LPS 5mg/kg after 6 hours group, LPS(5)6h+DIBI(@4h): LPS 5mg/kg after 6 hours and DIBI administration at time 4 hours post LPS instillation.

Lung	LPS (5)4h	DIBI(@0h)	DIBI(@2h)	DIBI(@4h)	LPS (5) 6h
LIX	↑	↓	↓	~~Θ~~	↑
CXCL2	↑	↓	↓	↓	↑
CCL5	↑	↓	↓	↓	↑
CXCL10	↑	~~Θ~~	~~Θ~~	~~Θ~~	↑
IL-1β	↑	~~Θ~~	~~Θ~~	~~Θ~~	↑
IL-6	↑	↓	↓	↓	↑
CXCL1	↑	~~Θ~~	~~Θ~~	~~Θ~~	↑

Table 3. Summary table for lung inflammatory mediators. In this table, DIBI treatment groups (DIBI @0h, @2h, and @4h) were compared to LPS (5)4h and LPS (5)6h, and LPS groups were compared to control groups. The symbols ~~Θ~~, ↑, ↓ represents no significant changes, significant increase, and significant decrease, respectively.

3.2.4. Plasma cytokines in presence of DIBI treatment

Four hours after administering 5mg/kg of LPS, plasma levels of CCL5, CXCL10, IL-6, and CXCL1 significantly increased, however, levels of LIX, CXCL2, IL-17 in plasma did not significantly increase relative to control group (CON4h). Administration of DIBI with dosage of 80 mg/kg at time 0 hour after LPS instillation and at time 2 hours post LPS instillation could not reduce the plasma levels of these inflammatory mediators: LIX, CXCL2, CCL5, CXCL10, IL-6, IL-17, and CXCL1 relative to LPS 5 mg/kg after 4 hours group (Figure8A-G, left panel). No remarkable different between early treatments with DIBI was observed.

The plasma level of CXCL2 still significantly increased 6 hours after administrating 5 mg/kg LPS. The levels of CCL5, CXCL10, IL-6, and CXCL1 in plasma, remained significantly high relative to control group (CON6h). DIBI treatment at time 4 hours post LPS instillation, could not reduce the plasma level of any of studied inflammatory mediators (LIX, CXCL2, CCL5, CXCL10, IL-6, IL-17, and CXCL1) relative to LPS 5 mg/kg after 6 hours group (Figure 8A-G, right panel). Plasma level of CXCL10, was significantly increased after DIBI administration at 4 hours post LPS instillation relative to LPS 6 hours group (Figure 8D, right panel).

Four hours and 6 hours after administering 5mg/kg of LPS, the plasma level of TNF-α was increased whereas it was undetectable in their respective control groups.

Plasma levels of IL-1β and IFN- γ were undetectable for all tested groups.

The changes in plasma levels of inflammatory mediators in our study was summarized in Table 4.

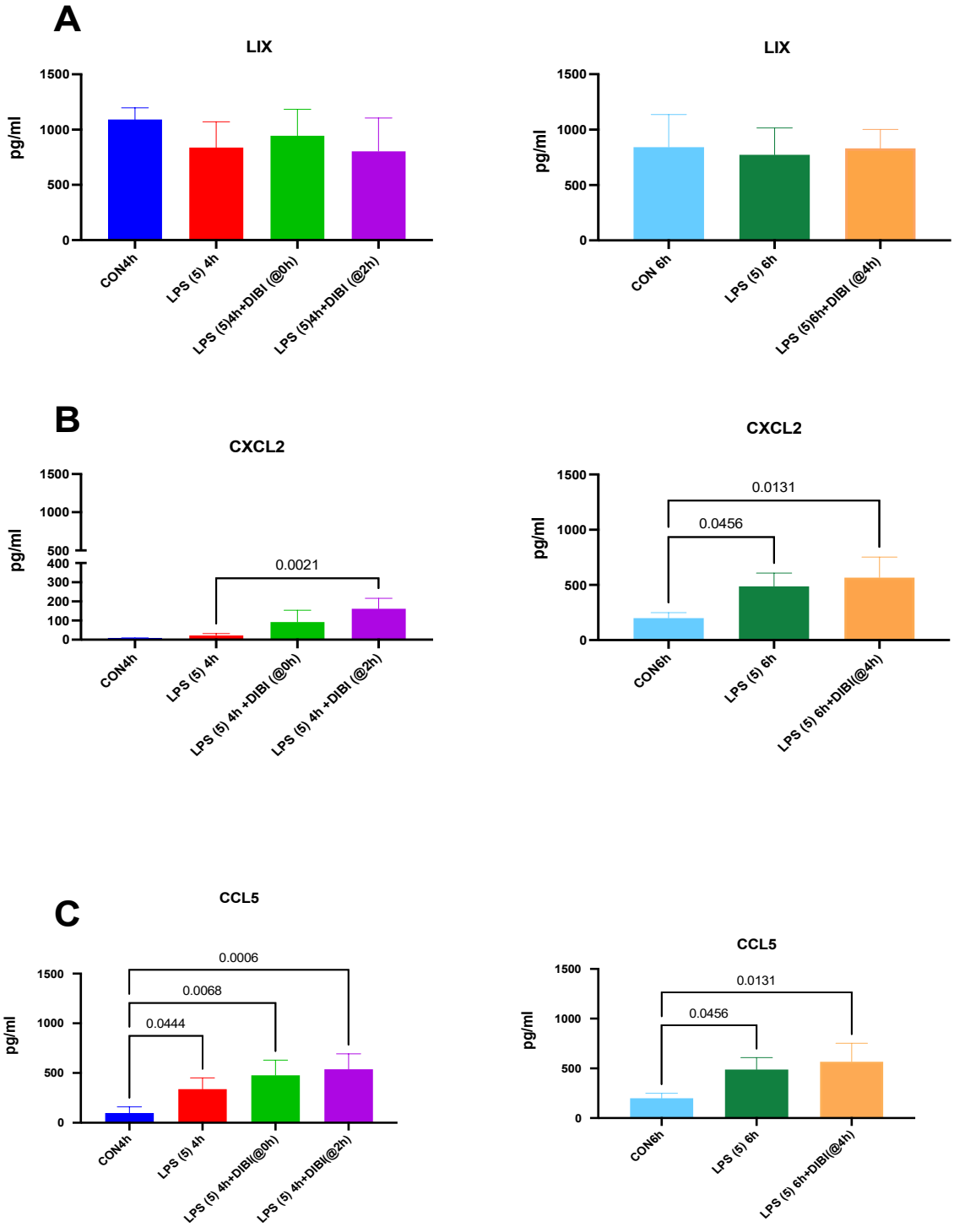
A
LIX
pg/ml
1500
1000
500
0
CON4h
LPS (5) 4h
LPS (5)4h+DIBI (@0h)
LPS (5)4h+DIBI (@2h)
LIX
pg/ml
1500
1000
500
0
CON 6h
LPS (5) 6h
LPS (5)6h+DIBI (@4h)
B
CXCL2
pg/ml
1500
1000
500
400
300
200
100
0
0.0021
CON4h
LPS (5) 4h
LPS (5) 4h +DIBI (@0h)
LPS (5) 4h +DIBI (@2h)
CXCL2
pg/ml
1500
1000
500
0
0.0131
0.0456
CON6h
LPS (5) 6h
LPS (5) 6h+DIBI(@4h)
C
CCL5
pg/ml
1500
1000
500
0
0.0006
0.0068
0.0444
CON4h
LPS (5) 4h
LPS (5) 4h+DIBI(@0h)
LPS (5) 4h+DIBI(@2h)
CCL5
pg/ml
1500
1000
500
0
0.0131
0.0456
CON6h
LPS (5) 6h
LPS (5) 6h+DIBI(@4h)

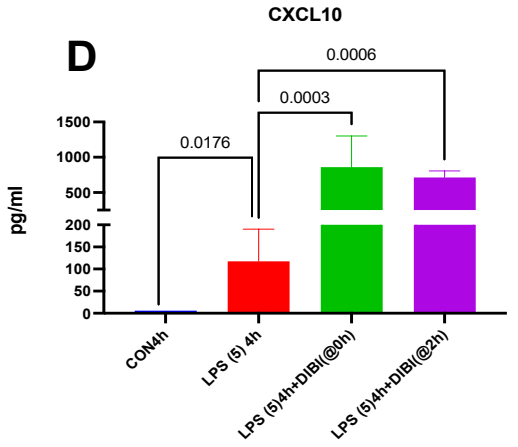
D
CXCL10
0.0006
0.0003
0.0176
pg/ml
1500
1000
500
200
150
100
50
0
CON4h
LPS (5) 4h
LPS (5)4h+DIBI(@0h)
LPS (5)4h+DIBI(@2h)

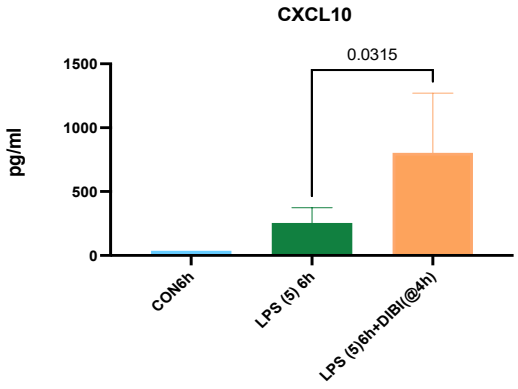
CXCL10
0.0315
pg/ml
1500
1000
500
0
CON6h
LPS (5) 6h
LPS (5)6h+DIBI(@4h)

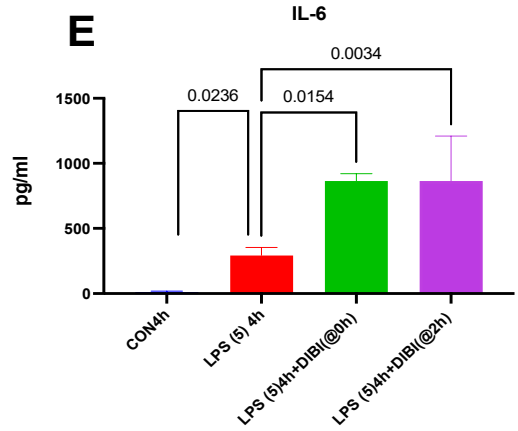
E
IL-6
0.0034
0.0236
0.0154
pg/ml
1500
1000
500
0
CON4h
LPS (5) 4h
LPS (5)4h+DIBI(@0h)
LPS (5)4h+DIBI(@2h)

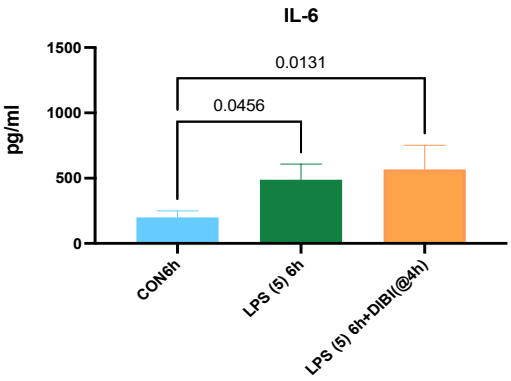
IL-6
0.0131
0.0456
pg/ml
1500
1000
500
0
CON6h
LPS (5) 6h
LPS (5) 6h+DIBI(@4h)

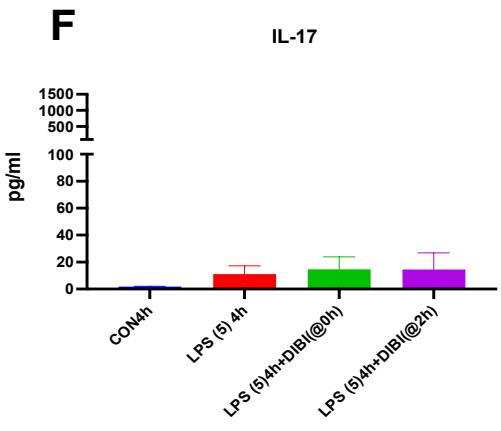
F
IL-17
pg/ml
1500
1000
500
100
80
60
40
20
0
CON4h
LPS (5) 4h
LPS (5)4h+DIBI(@0h)
LPS (5)4h+DIBI(@2h)

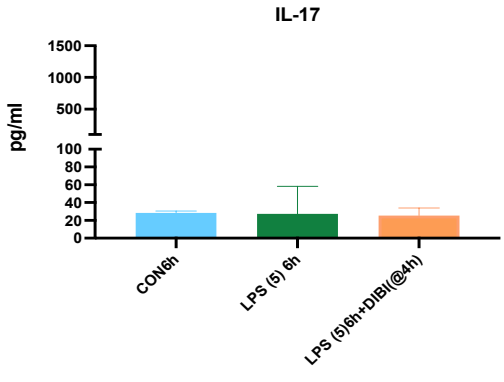
IL-17
pg/ml
1500
1000
500
100
80
60
40
20
0
CON6h
LPS (5) 6h
LPS (5)6h+DIBI(@4h)

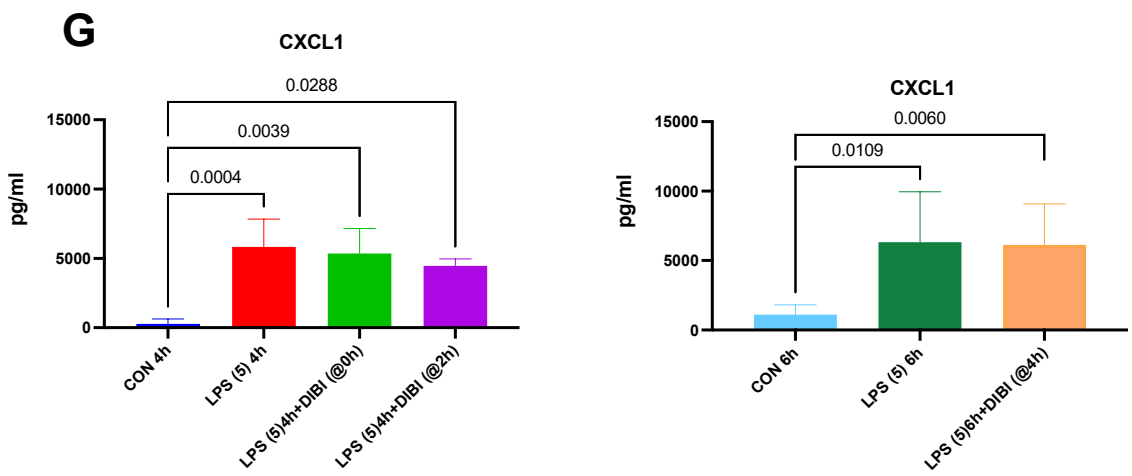

Figure 10. Effect of DIBI treatment on plasma inflammatory mediators. Early and Late treatment with DIBI (4 hours post-LPS 5 mg/kg instillation) could not significantly reduce the levels of inflammatory mediators in plasma (pg/ml). Data are expressed as means ± SD for each group (n = 5-9 mice per group), p values for significant differences are indicated on top of each comparison bars. CON4h: Control group after 4 hours Saline, LPS (5) 4h: LPS 5mg/kg after 4 hours group, LPS(5)4h+DIBI(@0h): LPS 5mg/kg after 4 hours and DIBI administration at time 0hour post LPS instillation, LPS(5)4h+DIBI(@2h): LPS 5mg/kg after 4 hours and DIBI administration at time 2hours post LPS instillation, CON6h: Control group after 6 hours Saline, LPS (5) 6h: LPS 5mg/kg after 6 hours group, LPS(5)6h+DIBI(@4h): LPS 5mg/kg after 6 hours and DIBI administration at time 4hours post LPS instillation.

Plasma	LPS (5)4h	DIBI(@0h)	DIBI(@2h)	DIBI(@4h)	LPS (5)6h
LIX	ϴ	ϴ	ϴ	ϴ	ϴ
CXCL2	↑	ϴ	↑	ϴ	↑
CCL5	↑	ϴ	ϴ	ϴ	↑
CXCL10	↑	↑	↑	↑	↑
IL-6	↑	↑	↑	ϴ	↑
IL-17	ϴ	ϴ	ϴ	ϴ	ϴ
CXCL1	↑	ϴ	ϴ	ϴ	↑

Table 4. Summary table for plasma inflammatory mediators. DIBI treatment groups (DIBI @0h, @2h, and @4h) were compared to LPS (5)4h and LPS (5)4h, and LPS groups were compared to control groups. The symbols ϴ, ↑, ↓ represents no significant changes, significant increase, and significant decrease, respectively.

Chapter 4: Discussion

4.1. Objective 1

The goal of the first objective was to evaluate activation of the immune response in our murine model of lung inflammation induced by two dosages of LPS from *P. aeruginosa* at different time points. LPS administration is an established experimental model to study lung inflammation in rodents (17,21). LPS, usually from *E. coli* (29), *P. aeruginosa* (64), or *K. pneumoniae* (65), has been used to induce immune response in the murine lung either through intranasal (14,20,64) or intratracheal (29,66) instillation or indirectly through intraperitoneal (67) and intravenous (20) injection. The most important and relevant features to be considered in an ALI model including histological evidence of tissue injury, disruption of the alveolar-capillary barrier, and inflammatory response, was presented in a review by Matute-Bello et al (68). In our model, these features were well characterized, and lung inflammation was evaluated by histological examination using H&E staining, measurements of NF-κB activation in lung tissue using western blotting, and measurement of plasma and lung inflammatory mediator levels using multiplex assay. We found that LPS from *P. aeruginosa* induces significant histopathological damage, NF-κB activation, as well as remarkable increase in lung inflammatory mediators' levels after 4 hours at dosage of 5 mg/kg.

4.1.1. Histology

The pathological hallmarks of lung inflammation induced by LPS instillation are edema, infiltration of inflammatory cells into alveolar space, and disruption of endothelial and

epithelial barriers of the lung (69,70). Interestingly, there is evidence that LPS could disrupt tight junction proteins since an *in vitro* study indicated that , ZO-1 protein was dramatically decreased after LPS (10μg/ml) administration in human bronchial epithelial cells (BEAS-2b) (71).

In this study, we found remarkable tissue damage 4 hours after intranasal instillation of 5 mg/kg LPS from *P. aeruginosa* relative to control animals receiving saline and relative to low dosage of LPS (1 mg/kg). Tissue inflammation in our study resolved 8 hours after LPS instillation. It should be noted that control group receiving saline after 8 hours in comparison to 4 hours time-point presented with some inflammation. This was interpreted as either due to the manipulation of the animal as the inhalation of saline liquid may interfere with normal breathing, or due to washing the microbiota from the nose along with other pathogens from the nostril into the lungs and resulting in lung inflammation. Nonetheless, no significant increase in inflammation was observed after 8hrs of LPS treatment.

It is worth mentioning that there are variable findings in the time scale for LPS-induced lung injury models in rodents. Similar results were found in previous studies showing that histological changes were more evident 4 hours after inhalation of 10 mg/ml LPS from *E. coli* than after 24 h (72). Our results are also in agreement with studies in rats were LPS from *P. aeruginosa* was administered, which showed significant increase in LPS-binding protein (LBP), immune cell recruitment, and MPO activity resulting from LPS after 4 hours (73,74). Liu *et al.* also demonstrated that 6 hours after intratracheal delivery of a sub-lethal dose of LPS (5 mg/kg) from *E. coli*, there was a remarkable lung inflammatory response, including significant interstitial infiltration of inflammatory cells and

thickening of the alveolar walls. Additionally, lung wet to dry ratio, an index for the assessment of lung permeability and lung edema as well as LDH activity, an indicator of tissue damage, showed a remarkable increase 6 hours post LPS instillation (29). However, the authors also demonstrated in another study that LPS administration from *E. coli* (5 mg/kg, i.t.) resulted in histopathological injury 12 hours after instillation (14), which was in agreement with the results from LPS-induced lung inflammation from a different serotype of *E.coli* in BALB/c mice (66). In addition, Lv *et al.* reported that 12 hours post 0.5 mg/kg *E. coli* LPS, a significant increase in histopathological changes and in MPO as well as MDA activity levels were induced in murine lung tissue. Increased MPO and MDA levels are related to the accumulation of neutrophils in the lung and excessive lipid peroxidation due to ROS accumulation (75). Another study using LPS from *P. aeruginosa* revealed significant increases in the relative lung wet weight over body weight which started 12 hours after intrapulmonary instillation and continued until 24 hours following LPS administration (76). These findings contradict our results since tissue inflammation in our study resolved 8 hours after LPS instillation. The different results could be due to the induction of lung inflammation with a different LPS serotype and mouse strain, and age used in different studies.

4.1.2. NF-κB activation

Activation of the transcription factor, NF-κB is a critical step in the acute inflammatory response. Previous *in vitro* studies suggested that most of the pulmonary NF-κB activation occurs in lung neutrophils during endotoxemia (77). Shenkar *et al.* confirmed this by conducting an *in vivo* study and demonstrated that activation of NF-κB containing both P65 and P50 subunits was increased in lung neutrophils, 1 hour after injection of

LPS from *E.coli*. The increases in lung NF-κB activation following endotoxemia were reduced in mice made neutropenic by administering either cyclophosphamide or anti-neutrophil antibodies, detected by electrophoretic mobility shift assay (EMSA) analysis (67,78). Additionally, in patients with ARDS, NF-κB activation is elevated in alveolar macrophages (79).

In this study, we used the anti-p65NF-κB antibody (65kD) for western blotting as a measure of NF-κB activation. We found that NF-κB activation was significantly increased in the lung tissue of mice 4 hours after receiving 5 mg/kg LPS compared to the control group and the 8 hours LPS 5mg/kg group. Our results are in agreement with another study where animals received 5 mg/kg LPS from *E. coli* intratracheally and showed increased levels of phosphorylated p65-NF-κB in the lung relative to control animals (66). Harada *et al.* studied the translocation of p65 into the nucleus of two human cholangiocarcinoma (CC) lines (HuCCTl and CCKSl), one hour after 1 μg/ml LPS administration, by NF-κB immunofluorescence staining. However, they found that pre-treatment of the cells with MG132 (indirect inhibitor of NF-κB) for one hour and then treated with 1 μg/ml LPS for 3 hours, prevented nuclear translocation and DNA-binding activity of NF-κB, detected by colorimetric assay (80).

In addition, several studies suggested a positive correlation between activation of NLRP3 inflammasome and NF-κB activation in the lung of mice with LPS-induced lung inflammation. Using western blot, they showed that LPS instillation induces NLRP3 inflammasome priming through promoting NF-κB activation following IκB degradation (14,29,75). Lui *et al.* indicated significant increase in NLRP3 inflammasome in the lung

of LPS-treated mice after 6 hours by western blot and immunofluorescent stains. Interestingly, reactive oxygen species (ROS) production is one of the most important regulatory factors in activation of NLRP3 inflammasome. However, Lui *et al.* measured MDA levels as marker of lipid peroxidation as well as SOD levels. They found that MDA levels rapidly increased, while SOD levels in lung tissues dramatically decreased in LPS-treated mice 6 hours post-LPS intratracheally instillation (29).

Furthermore, it has been reported that activation of TREM-1 (triggering receptor expressed on myeloid cells) enhances TLR responses which activate mitogen activated-protein kinases (MAPKs) and lead to activation of NF-κB (81,82). Sakai *et al.,* using live cell imaging of immortalized bone-marrow derived macrophage cell lines (iBMDM) which express an enhanced green fluorescent protein (EGFP)-tagged p65, indicated that the pattern of NF-κB dynamics and translocation time was not changed in TRIF-deficient macrophages relative to wild type cells, while it was delayed with an altered pattern in MyD88-deficient cells, in response to LPS administration. These findings confirmed that the primary driver for LPS-dependent NF-κB translocation to the nucleus is the MyD88 signalling pathway (83).

4.1.3. Inflammatory mediators in plasma and lung tissue

Activation of NF-κB results in the expression of inflammatory mediators involved in the pathogenesis of ARDS, such as TNF-α, IL-1β, IL-6, IL-8 (or its murine homolog, MIP-2, respectively) and ICAM-1 (79,84). ARDS mortality (up to about 40%, (85)) can be strongly predicted by elevated plasma levels of cytokines, e.g. IL-1β, IL-6 and tumor necrosis factor-α (TNF-α) (86,87). Additionally, IL-6 is involved in the formation of

lung edema and hyaline membranes through promoting VEGF-A expression, which increases endothelial cell permeability (88). The close relationship between NF-κB activation and the expression of proinflammatory cytokines was demonstrated in ventilator-induced lung injury (89). After translocation of NF-κB into the nucleus and binding to DNA, the genes encoding proinflammatory cytokines (TNF-α, IL-1β, IL-6), chemokines (MIP-1, MCP-1), adhesion molecules (ICAM, VCAM, E-Selectin) and iNOS were upregulated (25,89–91).

The levels of some inflammatory mediators in the plasma or lung tissue samples of our study were too low to be detectable by the used assay (Luminex®). IL-1β, IFN-γ, and TNF-α were under the detection threshold in our plasma samples, while in lung tissue samples the level of IFN-γ, and TNF-α, and IL-17 were too low to be detected. Jacobs *et al.* obtained different results in plasma with significantly increased levels of IL-6, TNF-α, and Monocyte Chemoattractant Protein 1 (MCP-1) using a cytometric bead array at 2 hours after intranasal inoculation with 10 μg LPS from *K. pneumoniae* (65). Since our plasma samples were analyzed 4 hours after LPS administration, some cytokines may be past their peak levels (92). E.g., TNF-α and IL-1β are very early inflammatory cytokines with a very short half-life which are released following inflammatory stimuli (93). Regarding lung tissues, it has been found that there is a time-dependent release of TNF-α into the BALF following inhalation of LPS. Faffe *et al.* reported that maximal levels of TNF-α were measured in the BALF 3 h after inhalation of 0.3 mg/ml and 10 mg/ml LPS from *E. coli,* while at the 1-hour timepoint TNF-α levels reached 50 % of its maximal level in BALF (94).

We also found that mice challenged with intranasal LPS (5 mg/kg) showed a significant elevation of plasma and lung levels of CXCL2 (MIP-2), CXCL10 (IP-10), IL-6, CXCL1 (KC) compared to the control group, and compared to the groups with low dose LPS (1mg/kg) 4 hours after LPS administration. In lung tissues, IL-1β levels were also remarkably increased with LPS at a dosage of 5 mg/kg after 4 hours. Our findings in plasma and lung levels of IL-6 are consolidated by a previous study in rats, which showed an increased level of IL-6 in both plasma and BALF by ELISA, and increased MPO activity after 4 hours intratracheal administration of 5 mg/kg LPS from *P. aeruginosa* (74). Ali *et al.* reported not only increased plasma levels of IL-6, but also increased levels of IL-1β and TNF-α post intraperitoneal administration of 5 mg/kg LPS (86) which is in discrepancy to our findings. This difference is most likely due to the different LPS administration route in our study (intranasal). Hu *et al.* reported significant increases of IL-6, IL-1β, and TNF-α in BALF by ELISA at 7 hours after LPS stimulation (95). However, Sakuma *et al.* did not find significant changes in serum levels of CXCL1 and CXCL2 after two days of LPS instillation (96). CXCL1(KC) and CXCL2 (MIP-2) are two major groups of chemokines that are secreted from the airway epithelium and the activated macrophages to recruit neutrophils (97). Interestingly, in several murine models of ARDS and lung injury, CXCL1 and CXCL2 are quantitative markers of damage and inflammation (98). Our opposite findings in the plasma level of these two chemokines might be due to the shorter observation time after LPS administration. At 8 hours post LPS instillation, our lung tissue levels of CXCL1 at both low (1mg/kg) and high (5 mg/kg) LPS dosages remained significantly elevated. This result is in line with other studies reporting peak levels of these two markers in BALF at

24 hours post LPS administration (98)(99). Our results for CXCL10 plasma levels is in agreement with several human and animal studies (100,101). CXCL10 levels in our lung samples showed a significant increase at 4 hours after LPS instillation at a dosage of 5 mg/kg, while at 8 hours after LPS instillation only LPS at dosage of 1mg/kg demonstrated significant increase relative to control group. Our findings in mice lung tissues are comparable with the CXCL10 levels in LPS-induced ARDS in BALF and lung samples in rats (101). CXCL10 is also known as interferon-γ inducible protein 10 (IP-10) which is a chemokine secreted by most immune cells such as neutrophils, eosinophils and monocytes and non-immune cells including epithelial and endothelial cells recruiting several inflammatory cells (i.e., neutrophils, T lymphocytes and NK cells) to the site of inflammation (102,103). Based on microarrays, it has been indicated that the CXCL10 gene is upregulated after LPS stimulation in acute lung injury. Furthermore, Lang *et al.* reported that CXCL10 contributes to the pathophysiology of ARDS induced by LPS (101).

We did not observe significant changes in the plasma levels of LIX and IL-17 post LPS instillation at neither time points nor dosages relative to control groups. However, in lung tissue samples, the levels of LIX were significantly increased 4 hours after intranasal administration of LPS 5 mg/kg compared to the control group, while IL-17 was too low to be detected. IL-17 is mainly secreted by T_h17 cells and to some extent by neutrophils that promote neutrophil recruitment to the lungs. Our findings are in agreement with low levels of IL-17 observed in experimental lung injury induced by intranasal administration of LPS from *E. coli* (96). However, Ding *et al.* reported significant increases in lung, BALF, and plasma levels of IL-17 in lung injury induced by intratracheal *E. coli* LPS

instillation (3 mg/kg) in mice at 6, 12, 24 hours (104). Other authors found that LIX was readily detectable in the lung but not plasma following LPS administration, suggesting that LIX expression is confined to the lung parenchyma (51). LIX is expressed by alveolar epithelial cells type II in response to LPS challenge and recruits neutrophils in response to lung injury (105).

Last but not least, we found that the CCL5 levels in plasma indicated a significant increase at 8 hours after 5 mg/kg LPS administration (delayed response) relative to control group, while the lung levels of CCL5 were significantly increased at 4 hours after 5 mg/kg LPS administration. Hoberstroh *et al.* also showed a significant increase in glomerular CCL5 mRNA in rats at 6 hours post intraperitoneal injection of LPS from E. coli (106). However, Johnston *et al.* reported that pulmonary CCL5 mRNA levels were unchanged at 2, 6, and 24 hours after inhalation of LPS (107). CCL5 is secreted by T-cells, macrophages, epithelial cells inducing by IFN- γ, TNFα, and IL-1. In addition, CCL5 is predominantly a chemoattractant for monocytes and lymphocytes (108).

In summary, there are some controversial findings among the results from our study and in other studies with regards to inflammatory mediator levels in plamsa and lung tissues after LPS administration. However, our data support the conclusion that LIX, CXCL2 (MIP-2), CCL5, CXCL10 (IP-10), IL-1β, IL-6, and CXCL1 (KC) play essential roles in our model of LPS-induced lung injury with peak levels at 4 hours after challenge with 5 mg/kg LPS.

4.2. Objective 2

According to previous studies, it has been shown that DIBI, in comparison to other iron chelators, exerts both anti-inflammatory and anti-bacterial effects due to its strong iron-binding capacity to remove iron from being available to pathogens (35,57,109). Although DIBI has been shown to have therapeutic effects in some local and systemic inflammatory models (57,109–112), the exact anti-inflammatory effects of DIBI on LPS-induced lung inflammation in mice and the molecular mechanisms involved in these effects are still poorly understood.

Therefore, after we established a robust and reproducible lung inflammation by endotoxin at a dosage of 5 mg/kg LPS following 4 hours of observation time, we aimed to study the effects of anti-inflammatory treatment using DIBI at several timepoints post LPS instillation. We chose early and later time points for the administration of DIBI: immediately post LPS inhalation (T0), 2 hours (T2) and 4 hours (T4) after LPS nasal instillation. The 2 and 4 hours timepoints were considered more clinically relevant. In this study, we tested one dosage of DIBI (80 mg/kg) according to previous studies published by our lab, and the administration route was intraperitoneally (113). The anti-inflammatory effects of DIBI in the lung were evaluated by histological examination of lung tissues using H&E staining, measurements of NF-κB activation in lung tissue lysates using western blotting, and measurement of plasma and lung inflammatory mediator levels using multiplex assays.

We have demonstrated for the first time, that i.p. injection of DIBI, 2 hours post LPS instillation, attenuated LPS-induced lung inflammation in mice, as supported by reduced

histopathological lung injury, prevention of NF-κB phosphorylation and suppressed production of pro-inflammatory cytokines in lung tissue. This is in agreement with *in vitro* study by Ali et al. (62). Although we found that DIBI treatment reduced the NF-κB activation *in vivo*, further studies are needed to investigate all possible mechanisms involved in this process.

4.2.1. Histology

We found that i.p. injection of DIBI at a dosage of 80 mg/kg at timepoint 0 and 2 hours after LPS instillation, significantly attenuated histopathological changes induced by LPS after 4 hours observation time. However, administration of DIBI with the same dosage, 4 hours after LPS instillation, did not significantly reduce the inflammation (observation time: 6 hours). Therefore, we suggest that at early stages, damage and inflammation in the lung tissue can be alleviated by DIBI treatment. However, 4 hours after LPS administration, lung tissue indicated remarkable histopathological injury relative to the control group. The efficacy of DIBI to reduce inflammation at a late stage, in which significant damage was manifested in lung tissue, was not significant.

Our histopathological findings are in agreement with other experimental models of inflammation. For instance, the small intestine was examined for mucosal lesions in experimental systemic inflammation (sepsis) induced by LPS. Thorburn *et al.* reported that administration of DIBI treatment reduced mucosal damage and improved histopathological changes in small intestine (109).

The effects of DIBI on various measurements of inflammation were also assessed in several other studies. Islam *et al.* revealed a significant reduction in leukocyte recruitment

and remarkable improvement of Functional Capillary Density (FCD) after DIBI administration in surgical sepsis using intravital microscopy (114). Lehmann *et al.* also reported similar findings in an endotoxemia model of sepsis after DIBI treatment (115). Proinflammatory signals induce ROS formation and expression of adhesion molecules, triggering leukocyte rolling and subsequent adhesion (116). Hence, reduction in leukocyte recruitment might be due to the antioxidant effect of iron chelation blocking iron-regulated ROS formation after DIBI administration (111). Additionally, inflammatory responses induced by LPS promote a reduction in FCD, which is responsible for two major changes: first, an increase in leukocyte-endothelial cell interactions, and second, an increase in permeability of the microvasculature (endothelial damage) resulting in the formation of edema (117).

Furthermore, the effect of other iron chelators in lung inflammation was investigated in the literature. For instance, Kono *et al.* indicated that pre-treatment with i.p. DFX reduced infiltration of cells and exudate in lung tissue caused by intratracheal administration of 5 mg/kg LPS. In addition, DFX alleviates acute lung inflammation by inhibiting neutrophil recruitment into lung tissues and neutrophil extracellular trap (NET) formation, which directly damages alveolar epithelium and endothelial cells (61). These findings confirm the anti-inflammatory effects of iron chelators in experimental lung inflammation.

4.2.2. NF-κB activation

The second method used in our study to assess anti-inflammatory effects of DIBI was the measurement of NF-κB activation in lung tissues by Western blotting. As outlined in

Objective 1, we saw a significant increase in NF-κB activation in lung tissues 4 hours after LPS instillation at dosage 5 mg/kg.

DIBI treatment at early stages (0 and 2 hours after LPS instillation) significantly diminished NF-κB activation compared to untreated LPS animals after 4 hours observation time. The strongest effect was seen when DIBI was administered immediately after LPS challenge (T=0h). NF-κB was almost at the level of control animals at the 4 hours timepoint. In order to evaluate the effects of DIBI treatment at later stage (4 hours after LPS inhalation), NF-κB activation in lung tissue was compared to another group of LPS-treated animals with 6 hours observation time. Interestingly, DIBI still remarkably reduced NF-κB activation, almost to the level of control at the 6 hours timepoint (CON6h).

To summarize, our findings indicate that DIBI administration at all timepoints (0, 2, and 4 hours) after LPS inhalation significantly attenuates NF-κB activation in lung tissue. This result may be related to the ROS reducing effects of iron chelation since NF-κB activation is redox-sensitive (118,119). However, these positive findings were not completely mirrored in the histological results, in particular at later timepoints. Most likely, some of the histological changes could not be reversed by the delayed DIBI treatment. This could also be related to the relative short half-life of DIBI (2hrs) and ip injection route.

Our findings are consistent with results of other studies with different iron chelators. Lin et al. reported that treatment of cultured rat hepatic macrophages (HMs) with an iron chelator, L1, prevented LPS-induced NF-κB activation (120). Another *in vitro* study by

Ali et al. showed that treatment with high doses of DIBI (100 or 200 μM) did prevent nuclear translocation of NF-κB P65 in CF15 cells challenged with LPS. Higher doses of DIBI which molecular size is too large to pass cell walls, mobilize intracellular iron by binding to extracellular iron, thereby reducing iron bioavailability for intracellular ROS generation and NF-κB activation (62). In addition, Li et al., in an experimental murine model of local inflammation assessed by immunohistochemistry and western blot analysis, indicated that DFO blocked LPS-induced nuclear translocation of p65 subunit of NF-κB, since DFO inhibited LPS-induced NADPH oxidase which mediated oxidative stress through increase in protein levels of the catalytic NADPH oxidase subunit, $p22^{phox}$ (49).

In a different setting, another study evaluated the effect of iron chelators on NF-κB activation in myelodysplastic cells and in leukemia cell lines (K562 and HL60) characterized by high basal NF-κB activity. Messa et al. reported that NF-κB inhibition by DFO in these cell lines was not observed with DFP (121) .

4.2.3. Lung and plasma cytokine levels

To further assess inflammation post DIBI treatment in our murine model, levels of inflammatory cytokines and chemokines were measured in lung and plasma collected 4 and 6 hours after intranasal LPS challenge. Similar to our findings in Objective 1, plasma and lung levels of some inflammatory mediators in the DIBI treatment groups were too low to be detected by the assay (Luminex®). IL-1β, IFN-γ, and TNF-α were under the detection threshold in plasma samples, while in lung samples the level of IFN-γ, IL-17, and TNF-α were too low to be detected.

In plasma, DIBI treatment neither at early treatment (0 and 2 hours post LPS instillation) nor later treatment (4 hours after LPS inhalation) could reduce the levels of LIX, CXCL2, CCL5, CXCL10, IL-6,1L-17, or CXCL1, respectively. However, Kim et al., using the iron chelator, di-2-pyridylketone-4,4-dimethyl-3-thiosemicarbazone (Dp44mT), reported that serum levels of IL-1β and TNF-α were reduced in a dose-dependent fashion in a murine experimental model of allergic rhinitis (122). Others studies using the FDA-approved iron chelators, DFO or DFX in endotoxemic humans, mice and rats indicated decreased LPS-induced activation of NF-κB, reduced levels of TNF-α, IL-6, IL-1β in plasma and lower levels of inflammatory parameters of liver injury (123–126). Additionally, our findings are in discrepancy to previous studies, where administration of DIBI in systemic inflammation attenuated the levels of plasma cytokines and adhesion molecules (112,115,127). Obviously, the administration routes of LPS and DIBI are critical and should be considered in interpretation of the results. In our study we administered LPS intranasally, which is different from intraperitoneal injection of LPS (115).

Unlike our results from plasma, early treatment with DIBI at time 0 and 2 hours post LPS instillation significantly reduced the lung tissue levels of LIX, CXCL2, CCL5, and IL-6. However, later treatment with DIBI at time 4 hours after LPS inhalation, significantly diminished only lung levels of CXCL2 and IL-6. Therefore, we can conclude that early treatment with DIBI is effective to alleviate most of studied tissue inflammatory mediators in our model, which is in agreement with our findings from histopathological changes and NF-κB activation in lung tissue. He et al. evaluated the effect of DFO on allergic events caused by ovalbumin (OVA)-induced lung inflammation exacerbated by

particulate matter less than 2.5μm (PM2.5) with LPS. They found that DFO did not suppress neutrophil-related responses (IL-1β, IL-6, TNF-α, KC, RANTES) in BALF (128). When comparing our lung inflammation model with DIBI treatment to their results, we observed the same result in the lung level of only IL-1β and CXCL1 (KC) after DIBI administration at both early and later stages as well as in lung level of CCL5 after DIBI treatment in later stage (at 4 hours after LPS instillation). In addition, we found that IL-6 levels in lung tissue were remarkably decreased in both early and later treatment with DIBI. Ali *et al.* also indicated that higher concentrations of DIBI reduced the apical secretion of IL-6 in LPS-stimulated CF15 cells (62). Furthermore, similar finding were reported in an *in vitro* study that higher concentrations of DFO inhibited the release of IL-1β from LPS-stimulated AMs of both smokers and non-smokers (129). It should be noted that during the time course of lung inflammation, other organs such as brain respond to lung inflammation and release cytokines and chemokines which are mixed up with other plasma cytokines. Hence plasma cytokines do not mirror the changes in lung tissue since the cytokines from the brain also contribute to the plasma level of cytokines in response to lung inflammation. Although DIBI alone did not induce any significant changes in plasma levels of inflammatory mediators, cytokines from other tissues are expected to contribute to the plasma cytokines measured after DIBI treatment.

4.3. Limitations and future directions

Some limitations can be identified in our study. First, considering the genetic and physiological differences between humans and mice (130), murine models are not substitutes for human models. However, they are valuable tools to gain a preliminary understanding of how a medication may function in clinical trials. In this context, we first studied the anti-inflammatory effect of DIBI immediately after LPS instillation. After finding promising results, more clinically relevant time points for DIBI treatment were selected. However, for both LPS instillation and DIBI treatment, we still had only a limited number of time points and dosages to study the inflammatory changes. Since mice have a faster metabolism and immune response than humans following a stimulus such as LPS (131), shorter time points such as 30 minutes, 1 hour, 2 hours, and 3 hours after LPS administration should be included in future experiments. Furthermore, we only tested two doses of LPS from *P. aeruginosa* (1 mg/kg and 5 mg/kg) and one dose of DIBI (80 mg/kg) based on previous literature. Therefore, future experiments should also test more doses of DIBI to potentially improve its efficacy as well as more frequent administration of DIBI, to compensate for its short half-life. Additionally, the administration route of DIBI in our study was through intraperitoneal injection, while the LPS was administered intranasally. Potentially, inhalation of aerosolized DIBI would be a more effective route of administration.

Another limitation of our model is that experiments were performed on healthy mature adult male mice aged 12–14-week-old. Although it has been shown that male mice demonstrated significantly greater airway responsiveness to LPS relative to females (132), it is helpful to investigate the inflammatory lung changes in female mice in future

experiments. In addition, mature adult mice show cumulative immune responses following LPS exposure compared to young mice (133). Therefore, the factors of age and sex should be regarded in the interpretation of the results.

Recent studies reported the possible therapeutic effects of iron chelators in patients with COVID-19 through preventing excessive inflammatory response and tissue damage by blocking free iron and inhibiting the oxygen radical formation and lipid peroxidation (134,135). In addition the possibility of therapeutic effect of iron chelators in cystic fibrosis disease was suggested and then proved by Aali et al. in an *in vitro* study. (62,136). The results of our study also suggest the potential therapeutic use of DIBI in systemic inflammation caused by SARS-CoV-2 or in cystic fibrosis through targeting the release of inflammatory mediators such as ROS and prevention of cytokine storm.

4.4. Conclusion

The present study investigated the impact of the novel iron chelator, DIBI, on immune responses in an experimental murine model of lung inflammation. First, we established an LPS-induced lung inflammation model, using intranasal administration of two different doses of LPS at two different observation time points. Second, to assess the anti-inflammatory properties of DIBI, we administered DIBI intraperitoneally in the early and later stages. It was the first time that DIBI was tested in an experimental murine model of lung inflammation. We found that DIBI indicated an anti-inflammatory effect by attenuated LPS-induced pulmonary histopathological injury, NF-κB activation, and inflammatory mediators in lung tissues. These results suggest that DIBI could be utilized

as a promising anti-inflammatory treatment for lung inflammation caused by Gram-negative bacteria.

References

1. Cherayil BJ. Iron and immunity: immunological consequences of iron deficiency and overload. Arch Immunol Ther Exp (Warsz). 2010;58(6):407–15.

2. Widmaier EP, Raff H, Strang KT. Vander's human physiology. Vol. 5. McGraw-Hill New York, NY; 2006.

3. Lutfi MF. The physiological basis and clinical significance of lung volume measurements. Multidiscip Respir Med. 2017;12(1):1–12.

4. Levitzky MG. Pulmonary physiology. : McGraw-Hill Education,; 2018.

5. Hartl D, Tirouvanziam R, Laval J, Greene CM, Habiel D, Sharma L, et al. Innate immunity of the lung: from basic mechanisms to translational medicine. J Innate Immun. 2018;10(5–6):487–501.

6. Thompson AB, Robbins RA, Romberger Dj, Sisson JH, Teschler H, Rennard SI. Immunological functions of the pulmonary epithelium. Eur Respir J. 1995;8(1):127–49.

7. Bienenstock J. The lung as an immunologic organ. Annu Rev Med. 1984;35(1):49–62.

8. Martin TR, Frevert CW. Innate immunity in the lungs. Proc Am Thorac Soc. 2005;2(5):403–11.

9. Ingbar DH. Fishman's pulmonary diseases and disorders. Ann Am Thorac Soc. 2015;12(8):1255–6.

10. Iwasaki A, Foxman EF, Molony RD. Early local immune defences in the respiratory tract. Nat Rev Immunol. 2017;17(1):7–20.

11. Lloyd CM, Marsland BJ. Lung homeostasis: influence of age, microbes, and the immune system. Immunity. 2017;46(4):549–61.

12. McCormack V, Tolhurst-Cleaver S. Acute respiratory distress syndrome. Bja Educ. 2017;17(5):161–5.

13. Millar FR, Summers C, Griffiths MJ, Toshner MR, Proudfoot AG. The pulmonary endothelium in acute respiratory distress syndrome: insights and therapeutic opportunities. Thorax. 2016;71(5):462–73.

14. Dong L, Zhu Y-H, Liu D-X, Li J, Zhao P-C, Zhong Y-P, et al. Intranasal application of budesonide attenuates lipopolysaccharide-induced acute lung injury by suppressing nucleotide-binding oligomerization domain-like receptor family, pyrin domain-containing 3 inflammasome activation in mice. J Immunol Res. 2019;2019.

15. Pittet JF, Mackersie RC, Martin TR, Matthay MA. Biological markers of acute lung injury: prognostic and pathogenetic significance. Am J Respir Crit Care Med. 1997;155(4):1187–205.

16. Heflin AC, Brigham KL. Prevention by granulocyte depletion of increased vascular permeability of sheep lung following endotoxemia. J Clin Invest. 1981;68(5):1253–60.

17. Matute-Bello G, Frevert CW, Martin TR. Animal models of acute lung injury. Am J Physiol Cell Mol Physiol. 2008;295(3):L379–99.

18. Opal SM. Endotoxins and other sepsis triggers. In: Endotoxemia and Endotoxin Shock. Karger Publishers; 2010. p. 14–24.

19. Park BS, Lee J-O. Recognition of lipopolysaccharide pattern by TLR4 complexes. Exp Mol Med. 2013;45(12):e66–e66.

20. Szarka RJ, Wang N, Gordon L, Nation PN, Smith RH. A murine model of pulmonary damage induced by lipopolysaccharide via intranasal instillation. J Immunol Methods. 1997;202(1):49–57.

21. Domscheit H, Hegeman MA, Carvalho N, Spieth PM. Molecular dynamics of lipopolysaccharide-induced lung injury in rodents. Front Physiol. 2020;11:36.

22. Cardoso PG, Macedo GC, Azevedo V, Oliveira SC. Brucella spp noncanonical LPS: structure, biosynthesis, and interaction with host immune system. Microb Cell Fact. 2006;5(1):1–11.

23. Sander HD. Lipopolysaccharide recognition, internalisation, signalling and other cellular effects./H. Sander. Journ Endotoxin Res. 2001;7(5):335–48.

24. Aderem A, Ulevitch RJ. Toll-like receptors in the induction of the innate immune response. Nature. 2000;406(6797):782.

25. Srivastava SK, Ramana K V. Focus on molecules: nuclear factor-kappaB. Exp Eye Res. 2009;88(1):2.

26. Hariharan A, Hakeem AR, Radhakrishnan S, Reddy MS, Rela M. The role and therapeutic potential of NF-kappa-B pathway in severe COVID-19 patients. Inflammopharmacology. 2020;1–10.

27. Liu T, Zhang L, Joo D, Sun S-C. NF-κB signaling in inflammation. Signal Transduct Target Ther. 2017;2(1):1–9.

28. Lawrence T. The nuclear factor NF-κB pathway in inflammation. Cold Spring Harb Perspect Biol. 2009;1(6):a001651.

29. Liu T, Zhou Y, Li P, Duan J-X, Liu Y-P, Sun G-Y, et al. Blocking triggering receptor expressed on myeloid cells-1 attenuates lipopolysaccharide-induced acute lung injury via inhibiting NLRP3 inflammasome activation. Sci Rep. 2016;6(1):1–12.

30. Liu Q, Lv H, Wen Z, Ci X, Peng L. Isoliquiritigenin activates nuclear factor erythroid-2 related factor 2 to suppress the NOD-like receptor protein 3 inflammasome and inhibits the NF-κB pathway in macrophages and in acute lung injury. Front Immunol. 2017;8:1518.

31. Lu Z, Ou J, Cao H, Liu J, Yu L. Heat-Clearing Chinese Medicines in Lipopolysaccharide-Induced Inflammation. Chin J Integr Med. 2020;26(7):552–9.

32. Rietschel ET. Bacterial endotoxins: chemical structure, biological activity and role in septicaemia. Scand J Infect Dis Suppl. 1982;3:8.

33. Puig S, Ramos-Alonso L, Romero AM, Martínez-Pastor MT. The elemental role of iron in DNA synthesis and repair. Metallomics. 2017;9(11):1483–500.

34. Kim J, Wessling-Resnick M. The role of iron metabolism in lung inflammation and injury. J Allergy Ther. 2012;3(Suppl 4).

35. Scott C, Arora G, Dickson K, Lehmann C. Iron Chelation in Local Infection. Molecules. 2021;26(1):189.

36. Fokam D, Dickson K, Kamali K, Holbein B, Colp P. Iron Chelation in Murine Models of Systemic Inflammation Induced by Gram-Positive and Gram- Negative Toxins. Antibiotics. 2020;9(283):1–15.

37. Crielaard BJ, Lammers T, Rivella S. Targeting iron metabolism in drug discovery and delivery. Nat Rev Drug Discov. 2017;16(6):400.

38. Gunshin H, Mackenzie B, Berger U V, Gunshin Y, Romero MF, Boron WF, et al. Cloning and characterization of a mammalian proton-coupled metal-ion transporter. Nature. 1997;388(6641):482–8.

39. Kohgo Y, Ikuta K, Ohtake T, Torimoto Y, Kato J. Body iron metabolism and pathophysiology of iron overload. Int J Hematol. 2008;88(1):7–15.

40. Zhou L, Zhao B, Zhang L, Wang S, Dong D, Lv H, et al. Alterations in cellular iron metabolism provide more therapeutic opportunities for cancer. Int J Mol Sci. 2018;19(5):1545.

41. Zhang V, Nemeth E, Kim A. Iron in lung pathology. Pharmaceuticals. 2019;12(1):30.

42. Knutson MD. Iron transport proteins: gateways of cellular and systemic iron homeostasis. J Biol Chem. 2017;292(31):12735–43.

43. Knutson MD, Oukka M, Koss LM, Aydemir F, Wessling-Resnick M. Iron release from macrophages after erythrophagocytosis is up-regulated by ferroportin 1 overexpression and down-regulated by hepcidin. Proc Natl Acad Sci. 2005;102(5):1324–8.

44. Laftah AH, Ramesh B, Simpson RJ, Solanky N, Bahram S, Schümann K, et al. Effect of hepcidin on intestinal iron absorption in mice. Blood. 2004;103(10):3940–4.

45. Ramey G, Deschemin J-C, Durel B, Canonne-Hergaux F, Nicolas G, Vaulont S. Hepcidin targets ferroportin for degradation in hepatocytes. Haematologica. 2010;95(3):501.

46. De Domenico I, Zhang TY, Koening CL, Branch RW, London N, Lo E, et al. Hepcidin mediates transcriptional changes that modulate acute cytokine-induced inflammatory responses in mice. J Clin Invest. 2010;120(7):2395–405.

47. Holbein BE, Mira de Orduña R. Effect of trace iron levels and iron withdrawal by chelation on the growth of Candida albicans and Candida vini. FEMS Microbiol Lett. 2010;307(1):19–24.

48. Kruzel ML, Actor JK, Radak Z, Bacsi A, Saavedra-Molina A, Boldogh I. Lactoferrin decreases LPS-induced mitochondrial dysfunction in cultured cells and in animal endotoxemia model. Innate Immun. 2010;16(2):67–79.

49. Li L, Frei B. Iron Chelation Inhibits NF-κB–Mediated Adhesion Molecule Expression by Inhibiting p22phox Protein Expression and NADPH Oxidase Activity. Arterioscler Thromb Vasc Biol. 2006;26(12):2638–43.

50. Ghio AJ. Disruption of iron homeostasis and lung disease. Biochim Biophys Acta (BBA)-General Subj. 2009;1790(7):731–9.

51. Neves J, Haider T, Gassmann M, Muckenthaler MU. Iron Homeostasis in the Lungs—A Balance between Health and Disease. Pharmaceuticals. 2019;12(1):5.

52. Ganz T, Nemeth E. Iron homeostasis in host defence and inflammation. Nat Rev Immunol. 2015;15(8):500–10.

53. Xiong S, She H, Tsukamoto H. Signaling role of iron in NF-kappa B activation in hepatic macrophages. In: Comparative Hepatology. BioMed Central; 2004. p. 1–4.

54. Ali MK, Kim RY, Karim R, Mayall JR, Martin KL, Shahandeh A, et al. Role of iron in the pathogenesis of respiratory disease. Int J Biochem Cell Biol. 2017;88:181–95.

55. Reid DW, Lam QT, Schneider H, Walters EH. Airway iron and iron-regulatory cytokines in cystic fibrosis. Eur Respir J. 2004;24(2):286–91.

56. Poggiali E, Cassinerio E, Zanaboni L, Cappellini MD. An update on iron chelation therapy. Blood Transfus. 2012;10(4):411.

57. Arora N, Caldwell A, Wafa K, Szczesniak A, Caldwell M, Al-Banna N, et al. DIBI, a polymeric hydroxypyridinone iron chelator, reduces ocular inflammation in local and systemic endotoxin-induced uveitis. Clin Hemorheol Microcirc. 2018;69(1–2):153–64.

58. Coombs MRP, Grant T, Greenshields AL, Arsenault DJ, Holbein BE, Hoskin DW. Inhibitory effect of iron withdrawal by chelation on the growth of human and murine mammary carcinoma and fibrosarcoma cells. Exp Mol Pathol. 2015;99(2):262–70.

59. Heli H, Mirtorabi S, Karimian K. Advances in iron chelation: an update. Expert Opin Ther Pat. 2011;21(6):819–56.

60. Mobarra N, Shanaki M, Ehteram H, Nasiri H, Sahmani M, Saeidi M, et al. A review on iron chelators in treatment of iron overload syndromes. Int J Hematol stem cell Res. 2016;10(4):239.

61. Kono M, Matsuhiroya S, Obuchi A, Takahashi T, Imoto S, Kawano S, et al. Deferasirox, an iron-chelating agent, alleviates acute lung inflammation by inhibiting neutrophil activation and extracellular trap formation. J Int Med Res. 2020;48(9):0300060520951015.

62. Aali M, Caldwell A, Li A, Holbein B, Chappe V, Lehmann C. DIBI, a novel polymeric iron chelator modulates IL-6 and IL-8 secretion from Cystic Fibrosis airway epithelial cells in response to endotoxin induction. J Cell Biotechnol. 2020;(Preprint):1–10.

63. del Carmen Parquet M, Savage KA, Allan DS, Ang MTC, Chen W, Logan SM, et al. Antibiotic-resistant Acinetobacter baumannii is susceptible to the novel iron-sequestering anti-infective DIBI in vitro and in experimental pneumonia in mice. Antimicrob Agents Chemother. 2019;63(9).

64. Pang Z, Junkins RD, Raudonis R, MacNeil AJ, McCormick C, Cheng Z, et al. Regulator of calcineurin 1 differentially regulates TLR-dependent MyD88 and TRIF signaling pathways. PLoS One. 2018;13(5):e0197491.

65. Jacobs MC, Lankelma JM, Wolff NS, Hugenholtz F, de Vos AF, van der Poll T, et al. Effect of antibiotic gut microbiota disruption on LPS-induced acute lung inflammation. PLoS One. 2020;15(11):e0241748.

66. Bittencourt-Mernak MI, Pinheiro NM, Santana FPR, Guerreiro MP, Saraiva-Romanholo BM, Grecco SS, et al. Prophylactic and therapeutic treatment with the flavonone sakuranetin ameliorates LPS-induced acute lung injury. Am J Physiol Cell Mol Physiol. 2017;312(2):L217–30.

67. Abraham E, Carmody A, Shenkar R, Arcaroli J. Neutrophils as early immunologic effectors in hemorrhage-or endotoxemia-induced acute lung injury. Am J Physiol Cell Mol Physiol. 2000;279(6):L1137–45.

68. Matute-Bello G, Downey G, Moore BB, Groshong SD, Matthay MA, Slutsky AS, et al. An official American Thoracic Society workshop report: features and measurements of experimental acute lung injury in animals. Am J Respir Cell Mol Biol. 2011;44(5):725–38.

69. Bhattacharya J, Matthay MA. Regulation and repair of the alveolar-capillary barrier in acute lung injury. Annu Rev Physiol. 2013;75:593–615.

70. Han S, Mallampalli RK. The acute respiratory distress syndrome: from mechanism to translation. J Immunol. 2015;194(3):855–60.

71. Lee TJ, Choi YH, Song KS. The PDZ motif peptide of ZO-1 attenuates Pseudomonas aeruginosa LPS-induced airway inflammation. Sci Rep. 2020;10(1):1–11.

72. Skerrett SJ, Martin TR, Chi EY, Peschon JJ, Mohler KM, Wilson CB. Role of the type 1 TNF receptor in lung inflammation after inhalation of endotoxin or Pseudomonas aeruginosa. Am J Physiol Cell Mol Physiol. 1999;276(5):L715–27.

73. Eutamene H, Theodorou V, Schmidlin F, Tondereau V, Garcia-Villar R, Salvador-Cartier C, et al. LPS-induced lung inflammation is linked to increased epithelial permeability: role of MLCK. Eur Respir J. 2005;25(5):789–96.

74. Lê BV, Khorsi-Cauet H, Bach V, Gay-Quéheillard J. Modulation of Pseudomonas aeruginosa lipopolysaccharide-induced lung inflammation by chronic iron overload in rat. FEMS Immunol Med Microbiol. 2012;64(2):255–64.

75. Lv H, Liu Q, Wen Z, Feng H, Deng X, Ci X. Xanthohumol ameliorates lipopolysaccharide (LPS)-induced acute lung injury via induction of AMPK/GSK3β-Nrf2 signal axis. Redox Biol. 2017;12:311–24.

76. Wieland CW, Siegmund B, Senaldi G, Vasil ML, Dinarello CA, Fantuzzi G. Pulmonary inflammation induced by Pseudomonas aeruginosa lipopolysaccharide, phospholipase C, and exotoxin A: role of interferon regulatory factor 1. Infect Immun. 2002;70(3):1352–8.

77. McDonald PP, Bald A, Cassatella MA. Activation of the NF-κB pathway by inflammatory stimuli in human neutrophils. Blood, J Am Soc Hematol. 1997;89(9):3421–33.

78. Shenkar R, Abraham E. Mechanisms of lung neutrophil activation after hemorrhage or endotoxemia: roles of reactive oxygen intermediates, NF-κB, and cyclic AMP response element binding protein. J Immunol. 1999;163(2):954–62.

79. Moine P, McIntyre R, Schwartz MD, Kaneko D, Shenkar R, Le Tulzo Y, et al. NF-kappaB regulatory mechanisms in alveolar macrophages from patients with acute respiratory distress syndrome. Shock. 2000;13(2):85–91.

80. Harada K, Ohira S, Isse K, Ozaki S, Zen Y, Sato Y, et al. Lipopolysaccharide activates nuclear factor-kappaB through toll-like receptors and related molecules in cultured biliary epithelial cells. Lab Investig. 2003;83(11):1657–67.

81. Hara H, Ishihara C, Takeuchi A, Imanishi T, Xue L, Morris SW, et al. The adaptor protein CARD9 is essential for the activation of myeloid cells through ITAM-associated and Toll-like receptors. Nat Immunol. 2007;8(6):619–29.

82. Bouchon A, Facchetti F, Weigand MA, Colonna M. TREM-1 amplifies inflammation and is a crucial mediator of septic shock. Nature. 2001;410(6832):1103–7.

83. Sakai J, Cammarota E, Wright JA, Cicuta P, Gottschalk RA, Li N, et al. Lipopolysaccharide-induced NF-κB nuclear translocation is primarily dependent on MyD88, but TNFα expression requires TRIF and MyD88. Sci Rep. 2017;7(1):1–9.

84. Stellari FF, Sala A, Ruscitti F, Buccellati C, Allen A, Risé P, et al. CHF6001 inhibits NF-κB activation and neutrophilic recruitment in LPS-induced lung inflammation in mice. Front Pharmacol. 2019;10:1337.

85. Bellani G, Laffey JG, Pham T, Fan E, Brochard L, Esteban A, et al. Epidemiology, patterns of care, and mortality for patients with acute respiratory distress syndrome in intensive care units in 50 countries. Jama. 2016;315(8):788–800.

86. Ali H, Khan A, Ali J, Ullah H, Khan A, Ali H, et al. Attenuation of LPS-induced acute lung injury by continentalic acid in rodents through inhibition of inflammatory mediators correlates with increased Nrf2 protein expression. BMC Pharmacol Toxicol. 2020;21(1):1–14.

87. Bhatia M, Moochhala S. Role of inflammatory mediators in the pathophysiology of acute respiratory distress syndrome. J Pathol A J Pathol Soc Gt Britain Irel. 2004;202(2):145–56.

88. Kubo K, Hanaoka M, Hayano T, Miyahara T, Hachiya T, Hayasaka M, et al. Inflammatory cytokines in BAL fluid and pulmonary hemodynamics in high-altitude pulmonary edema. Respir Physiol. 1998;111(3):301–10.

89. Ko Y-A, Yang M-C, Huang H-T, Hsu C-M, Chen L-W. NF-κB activation in myeloid cells mediates ventilator-induced lung injury. Respir Res. 2013;14(1):1–13.

90. Grilli M, Chiu JJ-S, Lenardo MJ. IMF-κB and rel: Participants in a multiform transcriptional regulatory system. Int Rev Cytol. 1993;143:1–62.

91. Baeuerle PA, Henkel T. Function and activation of NF-kappaB in the immune system. Annu Rev Immunol. 1994;12(1):141–79.

92. Bozinovski S, Jones J, Beavitt S-J, Cook AD, Hamilton JA, Anderson GP. Innate immune responses to LPS in mouse lung are suppressed and reversed by neutralization of GM-CSF via repression of TLR-4. Am J Physiol Cell Mol Physiol. 2004;286(4):L877–85.

93. Kany S, Vollrath JT, Relja B. Cytokines in inflammatory disease. Int J Mol Sci. 2019;20(23):6008.

94. Faffe DS, Seidl VR, Chagas PS, de Moraes VLG, Capelozzi VL, Rocco PR, et al. Respiratory effects of lipopolysaccharide-induced inflammatory lung injury in mice. Eur Respir J. 2000;15(1):85–91.

95. Hu X, Tian Y, Qu S, Cao Y, Li S, Zhang W, et al. Protective effect of TM6 on LPS-induced acute lung injury in mice. Sci Rep. 2017;7(1):1–10.

96. Sakuma M, Khan MAS, Yasuhara S, Martyn JA, Palaniyar N. Mechanism of pulmonary immunosuppression: extrapulmonary burn injury suppresses bacterial endotoxin-induced pulmonary neutrophil recruitment and neutrophil extracellular trap (NET) formation. FASEB J. 2019;33(12):13602–16.

97. Roche JK, Keepers TR, Gross LK, Seaner RM, Obrig TG. CXCL1/KC and CXCL2/MIP-2 are critical effectors and potential targets for therapy of Escherichia coli O157: H7-associated renal inflammation. Am J Pathol. 2007;170(2):526–37.

98. Lax S, Wilson MR, Takata M, Thickett DR. Using a non-invasive assessment of lung injury in a murine model of acute lung injury. BMJ Open Respir Res. 2014;1(1):e000014.

99. Rittirsch D, Flierl MA, Day DE, Nadeau BA, McGuire SR, Hoesel LM, et al. Acute lung injury induced by lipopolysaccharide is independent of complement activation. J Immunol. 2008;180(11):7664–72.

100. Watanabe T, Mitsuhashi M, Sagawa M, Ri M, Suzuki K, Abe M, et al. Lipopolysaccharide-Induced CXCL10 mRNA Level and Six Stimulant-mRNA Combinations in Whole Blood: Novel Biomarkers for Bortezomib Responses Obtained from a Prospective Multicenter Trial for Patients with Multiple Myeloma. PLoS One. 2015;10(6):e0128662.

101. Lang S, Li L, Wang X, Sun J, Xue X, Xiao Y, et al. CXCL10/IP-10 neutralization can ameliorate lipopolysaccharide-induced acute respiratory distress syndrome in rats. PLoS One. 2017;12(1):e0169100.

102. Romagnani P, Crescioli C. CXCL10: a candidate biomarker in transplantation. Clin Chim acta. 2012;413(17–18):1364–73.

103. Scolletta S, Colletti M, Di Luigi L, Crescioli C. Vitamin D receptor agonists target CXCL10: new therapeutic tools for resolution of inflammation. Mediators Inflamm. 2013;2013.

104. Ding Q, Liu G-Q, Zeng Y-Y, Zhu J-J, Liu Z-Y, Zhang X, et al. Role of IL-17 in LPS-induced acute lung injury: an in vivo study. Oncotarget. 2017;8(55):93704.

105. Jeyaseelan S, Chu HW, Young SK, Worthen GS. Transcriptional profiling of lipopolysaccharide-induced acute lung injury. Infect Immun. 2004;72(12):7247–56.

106. Haberstroh U, Pocock J, Gómez-Guerrero C, Helmchen U, Hamann A, Gutierrez-Ramos JC, et al. Expression of the chemokines MCP-1/CCL2 and RANTES/CCL5 is differentially regulated by infiltrating inflammatory cells. Kidney Int. 2002;62(4):1264–76.

107. Johnston CJ, Finkelstein JN, Gelein R, Oberdörster G. Pulmonary cytokine and chemokine mRNA levels after inhalation of lipopolysaccharide in C57BL/6 mice. Toxicol Sci. 1998;46(2):300–7.

108. Rabin RL. CC, C, and CX3C Chemokines. 2003;

109. Thorburn T, Aali M, Kostek L, LeTourneau-Paci C, Colp P, Zhou J, et al. Anti-inflammatory effects of a novel iron chelator, DIBI, in experimental sepsis. Clin Hemorheol Microcirc. 2017;67(3–4):241–50.

110. Hagn G, Holbein B, Zhou J, Lehmann C. Anti-inflammatory iron chelator, DIBI, reduces leukocyte-endothelial adhesion and clinical symptoms of LPS-induced interstitial cystitis in mice. 2021;

111. Lehmann C, Islam S, Jarosch S, Zhou J, Hoskin D, Greenshields A, et al. The utility of iron chelators in the management of inflammatory disorders. Mediators Inflamm. 2015;2015.

112. Islam S, Jarosch S, Zhou J, del Carmen Parquet M, Toguri JT, Colp P, et al. Anti-inflammatory and anti-bacterial effects of iron chelation in experimental sepsis. J Surg Res. 2016;200(1):266–73.

113. Thorburn T. Iron-related immune cell function in sepsis. 2019;

114. Islam S, Jarosch S, Zhou J, Parquet MDC, Toguri JT, Colp P, et al. Anti-inflammatory and anti-bacterial effects of iron chelation in experimental sepsis. J Surg Res. 2015;200(1):266–73.

115. Lehmann C, Aali M, Zhou J, Holbein B. Comparison of Treatment effects of different iron chelators in experimental models of sepsis. Life. 2021;11(1):57.

116. Vachharajani TJ, Work J, Issekutz AC, Granger DN. Heme oxygenase modulates selectin expression in different regional vascular beds. Am J Physiol Circ Physiol. 2000;278(5):H1613–7.

117. Sarelius IH, Kuebel JM, Wang J, Huxley VH. Macromolecule permeability of in situ and excised rodent skeletal muscle arterioles and venules. Am J Physiol Circ Physiol. 2006;290(1):H474–80.

118. Xiong S, She H, Sung CK, Tsukamoto H. Iron-dependent activation of NF-κB in Kupffer cells: a priming mechanism for alcoholic liver disease. Alcohol. 2003;30(2):107–13.

119. Gumbau-Brisa R, Ang MTC, Holbein BE, Bierenstiel M. Enhanced Fe 3+ binding through cooperativity of 3-hydroxypyridin-4-one groups within a linear co-polymer: wrapping effect leading to superior antimicrobial activity. BioMetals. 2020;33(6):339–51.

120. Lin M, Rippe RA, Niemela O, Brittenham G, Tsukamoto H. Role of iron in NF-kappa B activation and cytokine gene expression by rat hepatic macrophages. Am J Physiol Liver Physiol. 1997;272(6):G1355–64.

121. Messa E, Carturan S, Maffè C, Pautasso M, Bracco E, Roetto A, et al. Deferasirox is a powerful NF-κB inhibitor in myelodysplastic cells and in leukemia cell lines acting independently from cell iron deprivation by chelation and reactive oxygen species scavenging. Haematologica. 2010;95(8):1308.

122. Kim H-Y, Han N-R, Kim H-M, Jeong H-J. The iron chelator and anticancer agent Dp44mT relieves allergic inflammation in mice with allergic rhinitis. Inflammation. 2018;41(5):1744–54.

123. Wang S, Liu C, Pan S, Miao Q, Xue J, Xun J, et al. Deferoxamine attenuates lipopolysaccharide-induced inflammatory responses and protects against endotoxic shock in mice. Biochem Biophys Res Commun. 2015;465(2):305–11.

124. Vulcano M, Meiss RP, Isturiz MA. Deferoxamine reduces tissue injury and lethality in LPS-treated mice. Int J Immunopharmacol. 2000;22(8):635–44.

125. van Eijk LT, Heemskerk S, van der Pluijm RW, van Wijk SM, Peters WHM, van der Hoeven JG, et al. The effect of iron loading and iron chelation on the innate immune response and subclinical organ injury during human endotoxemia: a randomized trial. Haematologica. 2014;99(3):579.

126. Cermanova J, Kadova Z, Dolezelova E, Zagorova M, Safka V, Hroch M, et al. Deferoxamine but not dexrazoxane alleviates liver injury induced by endotoxemia in rats. Shock. 2014;42(4):372–9.

127. Fokam D, Aali M, Dickson K, Scott C, Holbein B, Zhou J, et al. The novel iron chelator, DIBI, attenuates inflammation and improves outcome in colon ascendens stent peritonitis-induced experimental sepsis. Clin Hemorheol Microcirc. 2020;(Preprint):1–21.

128. He M, Ichinose T, Yoshida S, Nishikawa M, Sun G, Shibamoto T. Role of iron and oxidative stress in the exacerbation of allergic inflammation in murine lungs caused by urban particulate matter< 2.5 μm and desert dust. J Appl Toxicol. 2019;39(6):855–67.

129. Blumer BM, Wesselius LJ. Differential regulation of human alveolar macrophage-derived interleukin-1β and tumor necrosis factor-α by iron. J Lab Clin Med. 1998;132(6):497–506.

130. Perlman RL. Mouse models of human diseaseAn evolutionary perspective. Evol Med public Heal. 2016;2016(1):170–6.

131. Mestas J, Hughes CCW. Of mice and not men: differences between mouse and human immunology. J Immunol. 2004;172(5):2731–8.

132. Card JW, Carey MA, Bradbury JA, DeGraff LM, Morgan DL, Moorman MP, et al. Gender differences in murine airway responsiveness and lipopolysaccharide-induced inflammation. J Immunol. 2006;177(1):621–30.

133. Gahima I, Twizeyimana E, LuckGonzales E, Remonde CG, Jeon SJ, Shin CY. Strain, Age, and Gender Differences in Response to Lipopolysaccharide (LPS) Animal Model of Sepsis in Mice. Yakhak Hoeji. 2021;65(1):17–22.

134. Vlahakos VD, Marathias KP, Arkadopoulos N, Vlahakos D V. Hyperferritinemia in patients with COVID-19: An opportunity for iron chelation? Artif Organs. 2021;45(2):163–7.

135. Perricone C, Bartoloni E, Bursi R, Cafaro G, Guidelli GM, Shoenfeld Y, et al. COVID-19 as part of the hyperferritinemic syndromes: the role of iron depletion therapy. Immunol Res. 2020;1–12.

136. Aali M, Caldwell A, House K, Zhou J, Chappe V, Lehmann C. Iron chelation as novel treatment for lung inflammation in cystic fibrosis. Med Hypotheses. 2017;104:86–8.

Appendices

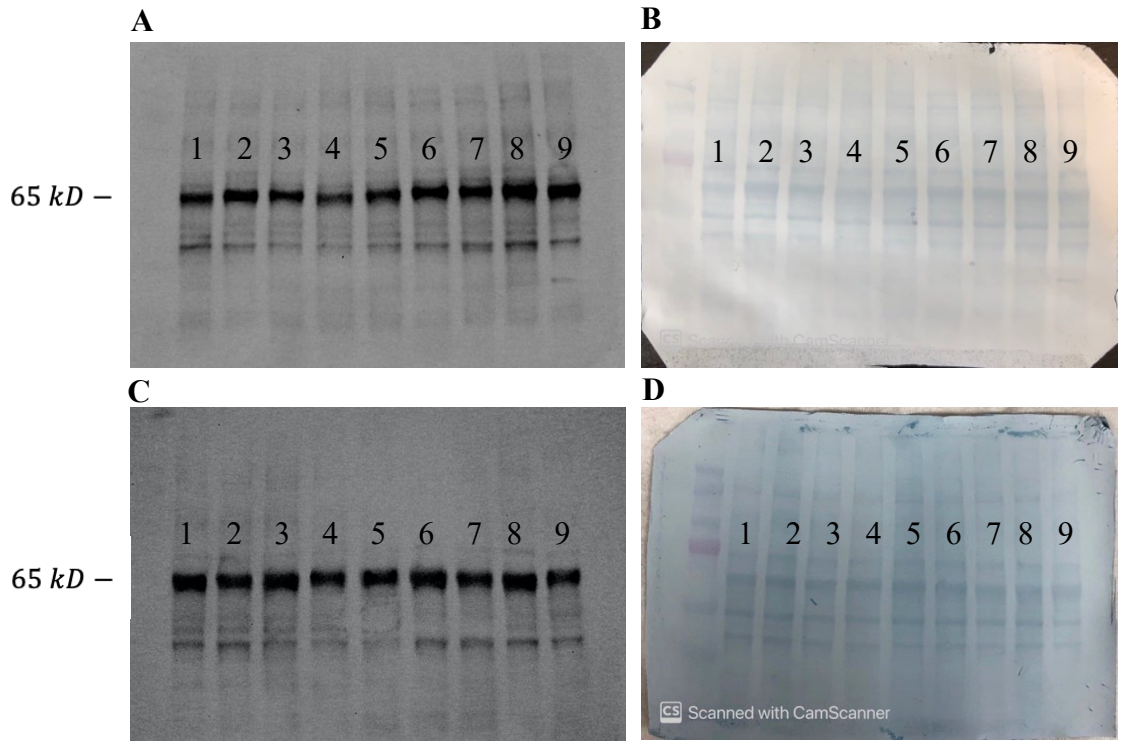

Figure A.1. Normalization of western blots with Amido black staining of total protein. Lanes 1 to 4 in Figure A.1.A are LPS 5 mg/kg after 4 hours+ DIBI 80 mg/kg at time 0 h(T0), while lanes 5 to 9 in Figure A.1.A are LPS 5 mg/kg after 4 hours+ DIBI 80 mg/kg at time 4 (T4). In Figure A.1.C, lanes 1 to 9 are LPS 5 mg/kg after 4 hours. Figures A.1.B&D are corresponding total protein-stained membrane with amido black.